AEROSPACE RESEARCH • AERODYNAMICS • PROPULSION • STRUCTURAL DYNAMICS • ELECTRONIC SYSTEMS AND INSTRUMENTS • COMPUTER MODULES

RESEARCH
ENGINEERING
PRODUCTION

MIXING IN SUPERSONIC FLOW

GASL TECHNICAL REPORT NUMBER 592

by:

J. H. Morgenthaler

GENERAL APPLIED SCIENCE LABORATORIES, INC.
MERRICK and STEWART AVENUES, WESTBURY, L.I., N.Y. · (516) ED 3-6960

Project 8027
Contract #NAS8-20066

COPY # 7

MIXING IN SUPERSONIC FLOW

GASL TECHNICAL REPORT # 592

by

J. H. Morgenthaler

Prepared for

National Aeronautical & Space Administration
George C. Marshall Space Flight Center
Huntsville, Alabama

Prepared by

General Applied Science Laboratories, Inc.
Merrick & Stewart Avenues
Westbury, L.I.,N.Y.

Approved by: A. Ferri
President

September 1966

SUMMARY

A method was presented for the determination of turbulent transport coefficients in multicomponent flows which requires a single differentiation of experimental $\overline{Y}$, $\overline{V}_z$, $\overline{H}$, and $\overline{\rho}$ data. Assumptions which allow simplification of the general equations of change, i.e., continuity, diffusion, momentum, and energy equations, without the restriction that $\partial\overline{P}/\partial r = 0$ were discussed. A constant stagnation temperature was shown to be a particular solution of the energy equation when Le_T and Pr_T (and hence Sc_T) are unity.

Limitations of the method were investigated using a test case, in which assumed values of the transport coefficients were used to generate downstream $\overline{Y}$ and $\overline{V}_z$ profiles, and these computed profiles then used in an attempt to reproduce the originally assumed transport coefficients. This technique allowed direct comparison of derived coefficients with the input values. Results of these comparisons showed the spacing of the data points to be a critical parameter, but that interpolated values could be used in conjunction with original data points (if properly smoothed). For the test case, in which the radius of the mixing region considered was 2 in., point spacings of 0.02 in. appeared sufficiently close to yield reasonable results; whereas, spacings of 0.06 in. did not.

An estimate of the turbulent transport coefficients for the case of coaxial free-jet mixing of subsonic hydrogen with Mach 1.6 air was obtained, using data of Reference 8, as an application of the method presented herein.

TABLE OF CONTENTS

LIST OF FIGURES

LIST OF TABLES

NOMENCLATURE

a	Arbitrary constant used to shift origin for Laurent series, ft
C_{p_i}	Specific heat at constant pressure, ft-lbf/lbm-$^\circ$R
D_i	Molecular diffusivity, or diffusion coefficient, ft^2/sec
E_{d_i}	Eddy diffusivity of mass, ft^2/sec
E_h	Eddy diffusivity of heat, ft^2/sec
E_m	Eddy diffusivity of momentum, ft^2/sec
f	Arbitrary constant used in Laurent series
g_c	Dimensional constant, 32.174 lbm-ft/lbf-sec^2
H	Stagnation enthalpy, ft-lbf/lbm
h	Static enthalpy, ft-lbf/lbm
k_n	Total mass flow rate within nth stream tube divided by 2π (defined by Equation (12)), lbm/sec
Le_i	Lewis number, $\bar{\rho} C_p D_i/k$
Le_{T_i}	Turbulent Lewis number, E_{d_i}/E_h
M	Mach number
P	Static pressure, lbf/ft^2
Pr	Prandtl number, $C_p \mu/k$
Pr_T	Turbulent Prandtl number, E_m/E_h
r	Radial coordinate, ft
r^*	Coordinate of wall or centerline, ft
r_s	Radial coordinate of streamline, ft
Sc_i	Schmidt number, $\mu/\rho D_i$
Sc_{T_i}	Turbulent Schmidt number, E_m/E_{d_i}
T	Absolute temperature, $^\circ$R
V	Mass-average or bulk velocity, ft/sec

NOMENCLATURE (contd.)

Y_i	Mass fraction
z	Axial coordinate, ft
ϵ_3	Eddy viscosity, $\bar{\rho}E_m$, lbm/ft-sec
$\varkappa$	Eddy thermal conductivity, $\bar{\rho}C_pE_h$, ft-lbf/sec-ft-°R
μ	Molecular shear viscosity, lbm/ft-sec
ξ	Turbulent mass transfer coefficient, $\bar{\rho}E_d$, lbm/ft-sec
ρ	Density, lbm/ft^3
Φ	Dissipation function, ft-lbf/ft^3-sec
φ	Arbitrary function

Subscripts

e	External (air) stream
i	Particular molecular (or atomic) species
j	Jet (Hydrogen) stream
r	Radial component
s	Streamline
T	Turbulent
t	Total or stagnation
w	Wall
z	Axial component

Arrows denote vectors; bars time-averaged; and primes turbulent fluctuating quantities.

MIXING IN SUPERSONIC FLOW

I. INTRODUCTION

A basic understanding of turbulent mixing is important for a wide range of current applications, including supersonic combustion ramjet engines and flows about launch and reentry vehicles. For example in a supersonic combustor employing a diffusion flame where mixing is the controlling mechanism, prediction of the mixing is critical to an understanding of the combustion phenomenon. In a hydrogen fueled upper stage vehicle, in which hydrogen is vented during the launch phase, knowledge of the mixing is necessary for the evaluation of potential hazards to the vehicle.

Unfortunately, no formal theoretical development for predicting mixing in complex turbulent flows is currently available so that a phenomenological approach must be applied. Such approaches (e.g., Prandtl's mixing theory, Reichardt's inductive theory, and von Karman's similarity hypothesis) have been used over the years as a means for treating specific mixing problems[1]. More recently various eddy viscosity models have been proposed[2-5]. In some cases solution of turbulent mixing problems have been obtained by incorporating these models into a finite difference technique for solving the appropriate equations [2,6,7].

An alternative approach has been considered by several investigators in which experimental data are used to determine turbulent transport coefficients[8-11]. These coefficients generally are applicable only for the particular experimental conditions for which they have been determined. They are useful for evaluating the degree of mixing obtained with a particular test geometry, and for comparing different geometries and flow conditions; however, their major usefulness ultimately should be correlation of supersonic mixing data so that predictions can be made, at least within the range of variables of interest.

In References 8 and 9 the assumption was made that normalized cosine profiles adequately represented both concentration and velocity data at regions downstream of the potential core of a coaxial supersonic jet. These fitted profiles were differentiated twice and used in the determination of the transport coefficients. Although cosine profiles may reasonably well approximate experimental data in regions in which similarity between radial concentration profiles and between velocity profiles exists, Hinze[12] shows that true similarity does not exist for the general case considered in References 8 and 9, in which the velocity of the jet and the external stream are of the same general magnitude, i.e., their velocities are significantly different but neither stream is quiescent. Since cosine profiles are only an approximation for these data, slopes obtained by differentiating them might not adequately represent true local variations of the experimental data, and the validity of transport coefficients derived by this procedure must be questioned.

For this reason, an alternative approach was selected in References 10 and 11, in which transport coefficients were determined by a single numerical differentiation of experimental concentration, velocity, and density profiles obtained at three or more axial stations; this approach is not limited to regions where similarity exists in the flow. Polynomials were fitted through five closely spaced data points and the required derivatives obtained by differentiating the polynomial using a five-point, second-order running smoothing routine[13]. The need for evaluating second derivatives was overcome by integrating the equations of change once in the radial direction from a boundary to a streamline. Experimental results were limited to the case of sonic radial and axial injection of cold hydrogen through circumferential wall slots into cold Mach 2 and 3 air streams. The energy equation was not considered in detail in this investigation since measurements showed the stagnation temperature remained approximately constant throughout the mixing region. The validity of the resulting coefficients was tested using a numerical integration technique (Crank-Nicolson) in which the transport coefficients and radial velocity were used in solving the diffusion and axial momentum equations both separately and simultaneously. Agreement between computed and experimental concentration and velocity profiles at several downstream axial stations was considered satisfactory evidence that valid eddy coefficients had been derived from the experimental profiles. Of course, agreement between computed and experimental profiles merely demonstrates the consistency of the eddy coefficients with the original profiles from which they were derived.

The analysis presented herein for coaxial injection is more general than that previously reported, since radial integration of the general axisymmetric diffusion and momentum equations as well as the simplified equations, and a detailed treatment of the energy equation are considered. In addition, analysis of a test case is presented which clarifies certain points of the numerical data handling techniques. In this test case, assumed values of the transport coefficients were used to generate downstream concentration and velocity profiles, and these computed profiles then used in an attempt to reproduce the originally assumed transport coefficients. Using this technique, the derived coefficients could be compared directly with the input values.

Unfortunately, no completely adequate experimental data were available for use for the determination of transport coefficients for the case of interest of supersonic, coaxial, free-jet mixing. However, experimental data presented in Reference 8, which generally contained five or six radial experimental data points at five or six axial stations, could be used as a first approximation if additional points were generated by interpolation. Analysis of these data is presented in the Appendix as an application of the method presented herein. Since any errors in the original points would be transmitted to the interpolated points, discrepancies in the original points would be magnified when the resulting profiles were differentiated. For this reason, no attempt was made to utilize these data for obtaining even an empirical mixing model; only simplified trends, suggested by smoothing the raw transport coefficients, were obtained. Fortunately, these trends were shown to be reasonably consistent with the original experimental data because computed and experimental concentration and velocity profiles agreed quite well at each downstream axial station at which experimental data were available. Of course closely-spaced accurate experimental data will be required in future work to obtain detailed variations and semiempirical models of the transport coefficients.

II. ANALYSIS

Generally, the starting point in turbulent analyses is the hypothesis that the Navier-Stokes equations and the other equations of change are satisfied by instantantaneous values of the velocity, concentration, and density. However, a group of French scientists recently has objected to this hypothesis; they feel that since a turbulent velocity field is in "pure chaos", the instantaneous velocity of a particle of fluid could not be sufficiently regular to satisfy a system of partial differential equations[14]. Of course, the same objection can be applied to use of the turbulent continuity, diffusion, and energy equations. Unfortunately, no substitute for these equations has been proposed, so that it is necessary to accept them as the starting point in turbulent analyses, at least as the best approximation available.

Pai[14] states that the final and logical solution of the turbulence problem will require application of the methods of statistical mechanics. This approach would require expressing the turbulent-transport rate of a transferable quantity completely in terms of statistical functions of the turbulent velocity field and of boundary or initial conditions. Until such a characterization is available, any solution of transport problems must be incomplete and at best approximate (i.e., semiempirical)[15]. Also before a rational statistical theory of turbulence can be developed along the lines of classical statistical mechanics, it is necessary that uniqueness and ergodic theorems be established as they have for the case of classical, statistical mechanics[14].

Since the Navier-Stokes equations are nonlinear, the proof of a general uniqueness theorem is extremely difficult, i.e., that a given initial state of a system at a particular time will uniquely determine its state at any other time. In experimental investigations time-average quantities, which depend on a particular ensemble, are used almost exclusively because in practice it is impossible to obtain statistical averages experimentally; however, in theoretical investigations statistical averages (i.e., ensemble averages) almost always are used. The ergodic theorem of classical statistical mechanics states the sufficient conditions for the equality of these two kinds of averages for almost all samples. Unfortunaely, no ergodic theorem has been proved in fluid mechanics; however, the assumption that two averages are equivalent is frequently made[14].

Therefore, in attacking practical turbulent mixing problems, instantaneous quantities are resolved into time-averaged and fluctuating quantities, substituted into the appropriate equations of change and time-averaged term-by-term. Some simplification of the resulting equations is obtained by assuming that in addition to fluctuations of velocity, density, pressure, and temperature (or enthalpy), there are fluctuations of mass flux [i.e., $(\rho\vec{V})$] regarded as a single property. This simplification, which allows the steady state continuity equation to be satisfied by both time-average and fluctuating components of the mass flux, was first employed by Van Driest in his analysis of turbulent compressible boundary layer flow (e.g. Reference 16). Application of these techniques to the steady, axisymmetric, equations of change yields*.

---

* Details of the method are presented in Reference 10.

Turbulent Continuity Equation

$$\frac{1}{r}\frac{\partial}{\partial r}\left(\overline{\rho V_r} r\right) + \frac{\partial}{\partial z}\left(\overline{\rho V_z}\right) = 0 \tag{1}$$

Turbulent Diffusion Equation

$$\overline{\rho V}_r \frac{\partial \bar{Y}_i}{\partial r} + \overline{\rho V}_z \frac{\partial \bar{Y}_i}{\partial z} = \frac{1}{r}\frac{\partial}{\partial r}\left[\bar{\rho}(D+E_{d_{i_1}})\, r \frac{\partial \bar{Y}_i}{\partial r}\right] + \frac{\partial}{\partial z}\left[\bar{\rho}(D+E_{d_{i_2}})\frac{\partial \bar{Y}_i}{\partial z}\right] \tag{2}$$

Turbulent Navier-Stokes Momentum Equations

a. Radial Equation

$$\overline{\rho V}_r \frac{\partial \bar{V}_r}{\partial r} + \overline{\rho V}_z \frac{\partial \bar{V}_r}{\partial z} = -g_c \frac{\partial \bar{P}}{\partial r} + \frac{2\mu}{r}\left(\frac{\partial \bar{V}_r}{\partial r} - \frac{\bar{V}_r}{r}\right) + \frac{2\epsilon_1}{3r}\left(2\frac{\partial \bar{V}_r}{\partial r} - \frac{\bar{V}_r}{r} - \frac{\partial \bar{V}_z}{\partial z}\right)$$
$$+ \frac{\partial}{\partial r}\left[\frac{2(\mu+\epsilon_1)}{3}\left(2\frac{\partial \bar{V}_r}{\partial r} - \frac{\bar{V}_r}{r} - \frac{\partial \bar{V}_z}{\partial z}\right)\right] + \frac{\partial}{\partial z}\left[(\mu+\epsilon_2)\left(\frac{\partial \bar{V}_z}{\partial r} + \frac{\partial \bar{V}_r}{\partial z}\right)\right] \tag{3}$$

b. Axial Equation

$$\overline{\rho V}_r \frac{\partial \bar{V}_z}{\partial r} + \overline{\rho V}_z \frac{\partial \bar{V}_z}{\partial z} = -g_c \frac{\partial \bar{P}}{\partial z} + \frac{1}{r}\frac{\partial}{\partial r}\left[(\mu+\epsilon_3) r\left(\frac{\partial \bar{V}_z}{\partial r} + \frac{\partial \bar{V}_r}{\partial z}\right)\right]$$
$$+ \frac{\partial}{\partial z}\left[\frac{2(\mu+\epsilon_4)}{3}\left(2\frac{\partial \bar{V}_z}{\partial z} - \frac{\bar{V}_r}{r} - \frac{\partial \bar{V}_r}{\partial r}\right)\right] \tag{4}$$

Turbulent Energy Equation

$$\overline{\rho V}_r \frac{\partial \bar{h}}{\partial r} + \overline{\rho V}_z \frac{\partial \bar{h}}{\partial z} + \frac{1}{r}\frac{\partial}{\partial r}\sum_i\left[\overline{(\rho V_r)'Y_i'}\, r\, \bar{h}_i + \overline{(\rho V_r)'h_i'}\, r\, \bar{Y}_i + \overline{(\rho V_r)'Y_i'h_i'}\, r\right]$$
$$+ \frac{\partial}{\partial z}\sum_i\left[\overline{(\rho V_z)'Y_i'}\,\bar{h}_i + \overline{(\rho V_z)'h_i'}\,\bar{Y}_i + \overline{(\rho V_z)'Y_i'h_i'}\right] = \frac{1}{r}\frac{\partial}{\partial r}\sum_i\left(kr\frac{\partial \bar{T}}{\partial r} + \bar{\rho} D_i r \bar{h}_i \frac{\partial \bar{Y}_i}{\partial r}\right.$$
$$+ D_i r\, \overline{\rho' h_i'}\frac{\partial \bar{Y}_i}{\partial r} + D_i r \bar{h}_i\, \overline{\rho' \frac{\partial Y_i'}{\partial r}} + \bar{\rho} D_i r\, \overline{h_i' \frac{\partial Y_i'}{\partial r}} + D_i r\, \overline{\rho' h_i' \frac{\partial Y_i'}{\partial r}}\Bigg) + \frac{\partial}{\partial z}\sum_i\left(k\frac{\partial \bar{T}}{\partial z}\right.$$
$$+ \bar{\rho} D_i \bar{h}_i \frac{\partial \bar{Y}_i}{\partial z} + D_i\, \overline{\rho' h_i'}\frac{\partial \bar{Y}_i}{\partial z} + D_i \bar{h}_i\, \overline{\rho' \frac{\partial Y_i'}{\partial z}} + \bar{\rho} D_i\, \overline{h_i' \frac{\partial Y_i'}{\partial z}} + D_i\, \overline{\rho' h_i' \frac{\partial Y_i'}{\partial z}}\Bigg) +$$
$$+ \bar{V}_r \frac{\partial \bar{P}}{\partial r} + \overline{V_r' \frac{\partial P'}{\partial r}} + \bar{V}_z \frac{\partial \bar{P}}{\partial z} + \overline{V_z' \frac{\partial P'}{\partial z}} + \bar{\Phi} \tag{5}$$

where

$$\overline{(\rho V_r)'Y_i'} \cong -\bar{\rho}E_{d_{i_1}} \frac{\partial \bar{Y}_i}{\partial r} \tag{6}$$

$$\overline{(\rho V_z)'Y_i'} \cong -\bar{\rho}E_{d_{i_2}} \frac{\partial \bar{Y}_i}{\partial z} \tag{7*}$$

$$\overline{(\rho V_r)'V_r'} \cong -\frac{2\epsilon_1}{3}\left(2\frac{\partial \bar{V}_r}{\partial r} - \frac{\bar{V}_r}{r} - \frac{\partial \bar{V}_z}{\partial z}\right) \tag{8}$$

$$\overline{(\rho V_z)'V_r'} \cong -\epsilon_2\left(\frac{\partial \bar{V}_z}{\partial r} + \frac{\partial \bar{V}_r}{\partial z}\right) \tag{9}$$

$$\overline{(\rho V_r)'V_z'} \cong -\epsilon_3\left(\frac{\partial \bar{V}_z}{\partial r} + \frac{\partial \bar{V}_r}{\partial z}\right) \tag{10}$$

$$\overline{(\rho V_z)'V_z'} \cong -\frac{2\epsilon_4}{3}\left(2\frac{\partial \bar{V}_z}{\partial z} - \frac{\bar{V}_r}{r} - \frac{\partial \bar{V}_r}{\partial r}\right) \tag{11}$$

Because of its complexity, Equation (5) is written in terms of Reynolds transport terms rather than turbulent transport coefficients; it must be simplified before it may be applied to practical problems. For the general case of subsonic flow and both subsonic and supersonic boundary layer flow, turbulent transport coefficients usually are defined so that the Reynolds transport terms can be replaced in the turbulent equations of change preserving the laminar form of these equations. Of course this substitution is arbitrary and really can be justified only if these coefficients prove to be a more useful representation than the original Reynolds transport terms. Because of the complexity of the momentum equations, four arbitrary coefficients of eddy viscosity were defined in order to preserve the laminar form of the equations.

---

* The axial dispersion coefficient is frequently defined in a similar manner to $E_{d_{i_2}}$.[17]

Unfortunately, at present no experimental procedure has been proposed for measuring the transport coefficients defined in Equations (6) to (11) directly. Of course, if one of the coefficients in each equation were considerably less important than the other, so that it could be neglected, each of the remaining terms in the equations might be evaluated using experimental data, and the missing coefficient determined. One integration of Equations (1) to (5) would eliminate the difficult task of obtaining accurate second derivatives of the experimental data. This result can be accomplished by integrating the equations once in the radial direction between a boundary and a streamline, i.e., a line bounding a fixed mass flow designated $r_s(n)$.

The values of $r_s(n)$ are found for a number of test-section lengths and various values of the constant k_n by a numerical evaluation of the integral

$$\int_{r^*}^{r_s(n)} \overline{\rho V_z}\, r dr = k_n \tag{12}$$

where r^* designates either the centerline or a streamline in the free stream. The boundary conditions at r^* are

$$r^* \begin{cases} o : \dfrac{\partial \bar{Y}_i}{\partial r} = \dfrac{\partial \bar{V}_z}{\partial r} = \dfrac{\partial r}{\partial z} = \dfrac{\partial \bar{H}}{\partial r} = \dfrac{\partial \bar{H}}{\partial z} = \bar{V}_r = 0 \\ \infty : \dfrac{\partial \bar{Y}_i}{\partial r} = \dfrac{\partial \bar{V}_z}{\partial r} = \dfrac{\partial \bar{Y}_i}{\partial z} = \dfrac{\partial \bar{V}_z}{\partial z} = \dfrac{\partial \bar{H}}{\partial r} = \dfrac{\partial \bar{H}}{\partial z} = 0 \end{cases} \tag{13}$$

since no mass, momentum, nor energy, diffuse in the free stream, and the centerline is an axis of symmetry. Equation (12) shows that there will be no net flux of mass across $r_s(n)$ by convection, although both fuel and air cross it by diffusion (equal masses in opposite directions).

Multiplying each term in the continuity equation, Equation (1), by rdr, integrating from either the free stream or the centerline to r_s and application of the generalized Liebnitz formula for interchanging the order of differentiation and integration yields

$$\left[\overline{\rho V_r} r_s\right]_{r_s} + \frac{\partial}{\partial z} \int_{r^*}^{r_s} \overline{\rho V_z}\, r dr = \left[\overline{\rho V_z} r_s \frac{\partial r_s}{\partial z}\right]_{r_s} \tag{14}$$

But Equation (12) requires that the second term on the left be zero, so that r_s

$$\overline{\rho V_r} = \overline{\rho V_z} \frac{\partial r_s}{\partial z} \tag{15}$$

Equations (2) to (4) may be integrated in a similar manner. Using Equation (15) there results

<u>Diffusion Equation</u>

$$\begin{aligned} &\frac{\partial}{\partial z} \int_{r^*}^{r_s} \left[\overline{\rho V_z}\, \bar{Y}_i - \bar{\rho}(D+E_{d_{i_2}}) \frac{\partial \bar{Y}_i}{\partial z}\right] r dr = \\ &= \left[\bar{\rho}\, (D+E_{d_{i_1}}) \frac{\partial \bar{Y}_i}{\partial r} - \bar{\rho}(D+E_{d_{i_2}}) \frac{\partial \bar{Y}_i}{\partial z} \frac{\partial r_s}{\partial z}\right]_{r_s} r_s \end{aligned} \tag{16}$$

<u>Radial Momentum Equation</u>

$$\begin{aligned} &\frac{\partial}{\partial z} \int_{r^*}^{r_s} \left[\overline{\rho V_z} \bar{V}_r - (\mu+\epsilon_2)\left(\frac{\partial \bar{V}_z}{\partial r} + \frac{\partial \bar{V}_r}{\partial z}\right)\right] r dr = \\ &+ \int_{r^*}^{r_s} \left[g_c \bar{P} - \frac{2\mu}{3}\left(2\frac{\bar{V}_r}{r} - \frac{\partial \bar{V}_r}{\partial r} - \frac{\partial \bar{V}_z}{\partial z}\right)\right] dr + \left[-g_c \bar{P} r\right]_{r^*}^{r_s} + \\ &+ \left[\frac{2(\mu+\epsilon_1)r}{3}\left(2\frac{\partial \bar{V}_r}{\partial r} - \frac{\bar{V}_r}{r} - \frac{\partial \bar{V}_z}{\partial z}\right) - (\mu+\epsilon_2) r \left(\frac{\partial \bar{V}_z}{\partial z} + \frac{\partial \bar{V}_r}{\partial z}\right)\frac{\partial r}{\partial z}\right]_{r^*}^{r_s} \end{aligned} \tag{17}$$

Axial Momentum Equation

$$\frac{\partial}{\partial z}\int_{r^*}^{r_s}\left[\overline{\rho V_z}\,\bar{V}_z + g_c\bar{P} - \frac{2(\mu+\epsilon_4)}{3}\left(2\,\frac{\partial\bar{V}_z}{\partial z} - \frac{\bar{V}_r}{r} - \frac{\partial\bar{V}_r}{\partial r}\right)\right] r\,dr =$$

$$\left[(\mu+\epsilon_3)\,r\left(\frac{\partial\bar{V}_z}{\partial r} + \frac{\partial\bar{V}_r}{\partial z}\right)\right]_{r^*}^{r_s} + \tag{18}$$

$$+ \left\{\left[g_c\bar{P} - \frac{2(\mu+\epsilon_4)}{3}\left(2\,\frac{\partial\bar{V}_z}{\partial z} - \frac{\bar{V}_r}{r} - \frac{\partial\bar{V}_r}{\partial r}\right)\right]\frac{\partial r}{\partial z}\,r\right\}_{r^*}^{r_s}$$

The momentum flux terms in Equations (17) and (18) are zero for the limit $r^* = 0$; however, they are not necessarily zero in the free stream because $\bar{V}_r$ can be finite, and therefore, $\partial r/\partial z \neq 0$.

Because of its complexity, Equation (5), the energy was not integrated until after the simplification discussed below. Fortunately, in cases where the stagnation temperature does not vary significantly in the mixing region, it is not necessary to consider the energy equation at all.

III. SIMPLIFIED ANALYSIS

Since six turbulent transport coefficients occur in Equations (15) to (18), there are insufficient equations available for their direct determination, even if all the remaining terms in these equations could be experimentally evaluated. To reduce the number of unknowns some assumptions must be made concerning their relationships, e.g., that some are either equal or negligible. Of course, even when such assumptions are made, accurate determination of the remaining terms would be difficult using experimental data because of the need to evaluate both axial and radial derivatives of various terms. An alternative approach to omitting terms, which leads to considerable simplification, is to make several general assumptions concerning the flow[10,11]. The assumptions that appear most reasonable for high-speed flow because of the importance of axially-directed convective bulk flow are:

1) Both diffusion and energy transfer in the axial direction by conduction and diffusion, are negligible compared to that in the radial direction;
2) Viscous normal stresses are negligible;
3) Viscous shear stresses depend primarily on the radial gradient of axial velocity $(\partial \bar{V}_z/\partial r >> \partial \bar{V}_r/\partial z)$;
4) The term $\overline{V_z(\partial P/\partial z)} >> \overline{V_r(\partial P/\partial r)}$

Assumtion 2) appears reasonable because an order of magnitude analysis shows viscous normal stresses are negligible compared to the pressure even in the boundary layer where viscous forces attain their maxima. A consequence of this assumption is $\overline{\rho V_z}\,\bar{V}_z >> \overline{(\rho V_z)'V_z'}$ which appears reasonable for high-speed flow and that $\overline{\rho V_r}\,\bar{V}_r >> \overline{(\rho V_r)'V_r'}$; it also allows simplification of the dissipation function $\bar{\Phi}$ which becomes

$$\overline{\Phi} \approx \frac{\mu}{g_c} \left[\left(\frac{\partial \overline{V}_z}{\partial r} \right)^2 + \left(\frac{\overline{\partial V'_z}}{\partial r} \right)^2 \right] \approx \frac{\mu}{g_c} \left(\frac{\partial \overline{V}_z}{\partial r} \right)^2 \tag{19}$$

If the additional reasonable assumption is made to simplify Equation (5) that terms containing $(\rho V_z)'$, ρ' and h' as products with other fluctuating terms are negligible,** Equations (2) to (5) become respectively,

Diffusion Equation*

$$\overline{\rho V}_r \frac{\partial \overline{Y}_i}{\partial r} + \overline{\rho V}_z \frac{\partial \overline{Y}_i}{\partial z} = \frac{1}{r} \frac{\partial}{\partial r} \left[\rho (D+E_{d_i}) r \frac{\partial \overline{Y}_i}{\partial r} \right] \tag{20}$$

Radial Momentum Equation

$$\overline{\rho V}_r \frac{\partial \overline{V}_r}{\partial r} + \overline{\rho V}_z \frac{\partial \overline{V}_r}{\partial z} = \frac{\partial}{\partial z} \left[(\mu + \epsilon_2) \frac{\partial \overline{V}_z}{\partial r} \right] - g_c \frac{\partial \overline{P}}{\partial r} \tag{21}$$

Axial Momentum Equation

$$\overline{\rho V}_r \frac{\partial \overline{V}_z}{\partial r} + \overline{\rho V}_z \frac{\partial \overline{V}_z}{\partial z} = \frac{1}{r} \frac{\partial}{\partial r} \left[(\mu + \epsilon_3) r \frac{\partial \overline{V}_z}{\partial r} \right] - g_c \frac{\partial \overline{P}}{\partial z} \tag{22}$$

Energy Equation

$$\overline{\rho V}_r \frac{\partial \overline{H}}{\partial r} + \overline{\rho V}_z \frac{\partial \overline{H}}{\partial z} = \frac{1}{r} \frac{\partial}{\partial r} \left[\left(\frac{k}{C_p} + \overline{\rho} E_h \right) r \frac{\partial \overline{H}}{\partial r} \right] +$$

$$+ \frac{1}{r} \frac{\partial}{\partial r} \sum_i \left\{ \left[D_i \left(1 - \frac{1}{Le_i}\right) + E_{d_i} \left(1 - \frac{1}{Le_{T_i}}\right) \right] r \overline{\rho} \overline{h}_i \frac{\partial \overline{Y}_i}{\partial r} \right\} + \tag{23}$$

$$+ \frac{1}{r} \frac{\partial}{\partial r} \left\{ \left[\mu \left(1 - \frac{1}{Pr}\right) + \overline{\rho} E_m \left(1 - \frac{1}{Pr_T}\right) \right] \frac{r}{2g_c} \frac{\partial \overline{V}_z^2}{\partial r} \right\}$$

where

$$\overline{(\rho V_z)' V_r'} \approx - \epsilon_2 \frac{\partial \overline{V}_z}{\partial r} \tag{24}$$

---

*In Equation (20) E_d has been written for E_{d_i}

**with the exception of $(\rho V_r)'$.

and

$$\overline{(\rho V_r)'V_z'} \approx - \epsilon_3 \frac{\partial \overline{V}_z}{\partial r} \tag{25}$$

These equations along with Equation (1) may be integrated as before to give

Continuity Equation

$$\overline{\rho V_r} = \overline{\rho V}_z \frac{\partial r_s}{\partial z} \tag{26}$$

Diffusion Equation

$$\frac{\partial}{\partial z} \int_{r*}^{r_s} \overline{\rho V}_z \overline{Y}_i \, rdr = [\, \overline{\rho} (D_i + E_{d_i}) r_s \frac{\partial \overline{Y}_i}{\partial r} \,]_{r_s} \tag{27}$$

Radial Momentum Equation

$$\frac{\partial}{\partial z} \int_{r*}^{r_s} [\overline{\rho V}_z \overline{V}_r - (\mu + \epsilon_2) \frac{\partial \overline{V}_z}{\partial r} \,] \, rdr = - \, [\, (\mu + \epsilon_2) r \frac{\partial \overline{V}_z}{\partial r} \frac{\partial r}{\partial z} \,]_{r*}^{r_s}$$

$$+ \int_{r*}^{r_s} g_c \overline{P} dr - [g_c \overline{P} r \,]_{r*}^{r_s} \tag{28}$$

Axial Momentum Equation

$$\frac{\partial}{\partial z} \int_{r*}^{r_s} \overline{\rho V}_z \overline{V}_z \, rdr = \left[(\mu + \epsilon_3) r \frac{\partial \overline{V}_z}{\partial r} \right]_{r*}^{r_s} + \left[g_c \overline{P} r \frac{\partial r}{\partial z} \right]_{r*}^{r_s}$$

$$- \frac{\partial}{\partial z} \int_{r*}^{r_s} g_c \overline{P} r \, dr \tag{29}$$

Energy Equation

$$\frac{\partial}{\partial z}\int_{r^*}^{r_s} \overline{\rho V_z}\,\overline{H}\; r dr = \left[\left(\frac{k}{C_p} + \overline{\rho}E_h\right) r\, \frac{\partial \overline{H}}{\partial r}\right]_{r_s} +$$

$$\sum_i \left\{\left[D_i\left(1-\frac{1}{Le_i}\right) + E_{d_i}\left(1-\frac{1}{Le_{T_i}}\right)\right] r_s \overline{\rho}\overline{h}_i\, \frac{\partial \overline{Y}_i}{\partial r}\right\}_{r_s} + \qquad (30)$$

$$\left\{\left[\mu\left(1-\frac{1}{Pr}\right) + \overline{\rho}E_m\left(1-\frac{1}{Pr_T}\right)\right] \frac{r_s \overline{V}_z}{g_c}\; \frac{\partial \overline{V}_z}{\partial r}\right\}_{r_s}$$

Since $\epsilon_2 \neq \epsilon_3$ unless $\overline{V}_r\overline{\rho' V_z'}$ and $\overline{V}_z\overline{\rho' V_r'}$ are small compared to $\overline{\rho}\overline{V_r' V_z'}$ or are approximately equal, each of these coefficients must be determined independently. However, the transfer of axial momentum is generally of greater interest than transfer of radial momentum, which may be quite small in applications such as free jet mixing; therefore, ϵ_2 frequently is of primary interest. Fortunately, it may be determined readily from Equation (29) and experimental $\overline{V}_z$, $\overline{\rho}$, and $\overline{P}$ profiles obtained at various axial stations, as long as the assumption is made that $\overline{\rho'\vec{V}'}$ is negligible compared to $\overline{\rho}\overline{\vec{V}}$. Note that there are no restrictions concerning radial pressure variations in Equations (22) and (29) as there are in the boundary layer momentum equation. If the viscous terms in Equations (21) and (28) are negligible, these equations still would be useful for checking the consistency of the inertial and pressure terms, and hence, the experimental measurements. If the inertial terms in these equations also were negligible, Equations (21) and (22) [and (28) and (29)] reduce to the usual boundary layer momentum equations, since in this case $\partial\overline{P}/\partial r=0$.

Equation (30) can be used to determine Pr_T and Le_{T_i} if experimental stagnation temperature profiles are available. Of course, for cases in which $\overline{T}_t$ was not constant throughout the flow, these profiles would be necessary for computation of $\overline{T}$, $\overline{\rho}$, and $\overline{V}_z$.

The stagnation enthalpy, $\overline{H}$ could be computed from $\overline{T}_t$ using the relation

$$\overline{H} = \int_{T_{ref}}^{\overline{T}_t} \sum_i C_{p_i} \overline{Y}_i \, d\overline{T}_t \tag{31}$$

Static enthalpies required in Equation (30) could be computed using the relations

$$\overline{h} = \overline{H} - \frac{\overline{V}_z^2}{2g_c} \tag{32}$$

and

$$\overline{h}_i = \overline{h} \, \overline{Y}_i \tag{33}$$

Since E_{d_i} and E_m are determined from Equation (27) and (29) Sc_{T_i} can be obtained from the relation $Sc_{T_i} = E_m/E_{d_i}$; Le_{T_i} can be eliminated from Equation (30) using the identity

$$Le_{T_i} \equiv Pr_T/Sc_{T_i} \tag{34}$$

and Equation (30) solved for Pr_T. Once Pr_T has been determined, Equation (34) can be used to compute Le_{T_i} completing the determination of the turbulent transport coefficients.

IV. PARTICULAR SOLUTION OF ENERGY EQUATION

The turbulent energy equation, Equation (23), can be rewritten in terms of the stagnation temperature, $\overline{T}_t$ by using the relations

$$\frac{\partial \overline{H}}{\partial r} = \frac{\partial}{\partial r}\left(\sum_i \overline{Y}_i \overline{H}_i\right) = \sum_i \overline{Y}_i \frac{\partial H_i}{\partial \overline{T}_t}\frac{\partial \overline{T}_t}{\partial r} + \sum_i \overline{H}_i \frac{\partial \overline{Y}_i}{\partial r} \qquad (35)$$

$$d\overline{H}_i = C_{p_i} d\overline{T}_t \qquad (36)$$

$$C_p = \sum_i C_{p_i} \overline{Y}_i \qquad (37)$$

which yields for the radial derivative

$$\frac{\partial \overline{H}}{\partial r} = C_p \frac{\partial \overline{T}_t}{\partial r} + \sum_i \overline{H}_i \frac{\partial \overline{Y}_i}{\partial r} \qquad (38)$$

Neglecting molecular transport compared to eddy transport for simplicity, substituting Equation (38) into Equation (23), and using a similar relation for the axial derivative, gives

$$C_p\left[\overline{\rho V}_r \frac{\partial \overline{T}_t}{\partial r} + \overline{\rho V}_z \frac{\partial \overline{T}_t}{\partial z}\right] = \frac{1}{r}\frac{\partial}{\partial r}\left[C_p \overline{\rho} E_h r \frac{\partial \overline{T}_t}{\partial r}\right] -$$

$$- \sum_i \overline{H}_i \left[\overline{\rho V}_r \frac{\partial \overline{Y}_i}{\partial r} + \overline{\rho V}_z \frac{\partial \overline{Y}_i}{\partial z} - \frac{1}{r}\frac{\partial}{\partial r}\left(\overline{\rho} E_h r \frac{\partial \overline{Y}_i}{\partial r}\right)\right] + \overline{\rho} E_h \sum_i C_{p_i} \frac{\partial \overline{Y}_i}{\partial r}\frac{\partial \overline{T}_t}{\partial r} + \qquad (39)$$

$$+ \frac{1}{r}\frac{\partial}{\partial r}\left[\sum_i \left(1 - \frac{1}{Le_{T_i}}\right) \overline{\rho} E_d r \overline{h}_i \frac{\partial \overline{Y}_i}{\partial r} + \left(1 - \frac{1}{Pr_T}\right) \overline{\rho} E_m \frac{r}{2g_c} \frac{\partial \overline{V}_z^2}{\partial r}\right]$$

If Le_{T_i} and Pr_T are unity, the second [see Equation (20)] and last terms on the right-hand-side of Equation (39) are identically zero; therefore, for this special case the energy equation becomes

$$c_p \left[\overline{\rho V}_r \frac{\partial \overline{T}_t}{\partial r} + \overline{\rho V}_z \frac{\partial T_t}{\partial z} \right] = \frac{1}{r} \frac{\partial}{\partial r} \left[c_p \overline{\rho} E_h r \frac{\partial \overline{T}_t}{\partial r} \right] + \qquad (40)$$

$$+ \overline{\rho} E_h \sum_i c_{p_i} \frac{\partial \overline{Y}_i}{\partial r} \frac{\partial \overline{T}_t}{\partial r}$$

Clearly, a constant $\overline{T}_t$ is a particular solution to this equation. Therefore, if $T_{t_o}(r)$ is constant at an initial axial station, Le_{T_i} and Pr_T (and therefore Sc_{T_i}) are unity, and the flow is adiabatic, the stagnation temperature will remain constant and equal to T_{t_o} throughout the flow field*. Note that $\overline{H}$ is not constant also, because $\overline{H}$ is a function of both the $\overline{Y}_i$'s and $\overline{H}_i$'s ($\overline{H}=\sum_i \overline{H}_i \overline{Y}_i$).

$\overline{T}_t$ in general can remain constant throughout the flow field only when Pr_T, Sc_{T_i}, and Le_{T_i} are unity; therefore, the procedure used in Reference 8 is again in general inconsistent, since $\overline{T}_t$ was assumed constant in the computation of $\overline{V}_z$ and $\overline{\rho}$, and these values then used for computing values of Sc_{T_i} and Le_{T_i} considerably different from unity.

---

* This result was first obtained from analysis of computer output; the analysis presented herein was undertaken at the suggestion of Dr. R. Edelman of GASL.

V. TEST OF NUMERICAL TECHNIQUE

The major difficulty in obtaining turbulent transport coefficients from experimental data is the evaluation of the axial derivatives of the integrals in Equations (27) to (30). In order to establish these derivatives, experimental profiles must be available at a minimum of three or four axial stations, so that a polynomial can be fitted and differentiated. The order of the polynomial can be up to one less than the number of axial stations available. However, the greater the order, the more frequent and extreme can be its oscillations and the more erratic the derivatives. Use of a lower order least squares fit would smooth the experimental data, but some of the resulting details of the distribution would be lost. Because adequate experimental profiles generally are not available at more than four or five axial stations, it is important to determine whether or not satisfactory axial derivatives can be obtained from such data. Therefore, a test case was prepared by assuming initial hydrogen concentration, and axial velocity profiles of the form

$$\overline{Y} = 0.45 + 0.45 \cos(2r) \tag{41}$$

$$\overline{V}_z = 1000 + 100r \tag{42}$$

where r varied from 0 to 2 inches (Figures 1 and 2). For simplicity, the stagnation temperature was assumed constant at the initial axial station because in many cold flow mixing studies, in which the stagnation temperature of the gases to be mixed are equal prior to mixing, measured stagnation temperatures vary only a few percent throughout the mixing region[8,10]. Also for simplicity, the static pressure was assumed equal to be atmospheric throughout the flow, and no radial momentum transfer was considered. Using a GASL program for the numerical integration of the diffusion, momentum, and energy equations[7], concentration, velocity, and density profiles were generated at numerous downstream stations, assuming a constant turbulent mass transfer coefficient, $\xi = \bar{\rho}E_d = 0.02$ lbm/ft-sec and Sc_T, Pr_T and Le_T to be unity*. Three computed concentration and velocity profiles at intervals of approximately 5 in. (in addition to the initial profiles) were selected for the test case; these profiles are presented in Figures 1 and 2.

The general geometry and profiles selected were similar to those used in Reference 18. These profiles were used as input to the computer program[10] developed for the determination of E_d and E_m (and ξ) which evaluates each term in Equations (27) and (29) and solves for the transport coefficients. Equation (28) was not used in the test case because radial momentum transfer had not been considered in the computation of the test profiles.

The integrals in Equations (12), (27), and (29) were evaluated numerically by interpolating the $\bar{Y}$, $\bar{V}_z$ and $\bar{\rho}$ profiles at 250 radial positions and using the trapezoidal rule; their axial variations were determinated by fitting a second order (for maximum smoothing) truncated Laurent polynomial in $f/(z+fa)$ and differentiating the polynomial.** The terms $\partial\bar{Y}/\partial r$ and $\partial\bar{V}_z/\partial r$ were determined by numerical differentiation of the concentration and velocity data, using a five-point, second-order, running-smoothing routine[13], and $\bar{\rho}$ was calculated from $\bar{Y}, \bar{V}_z$ and $\bar{T}$ using the perfect gas law and the assumption that $\bar{T}_t$ and $\bar{P}$ remained constant.

---

* The subscript i is dropped for the binary hydrogen-air system considered.

** f and a are constants which depend on the magnitude of the experimental range of z.

Results of these computations are presented in Figures 3 and 4. Unfortunately, the computer program used to generate the profiles in Figures 1 and 2 did not compute closely spaced grid points near the centerline because the stream function, Ψ, was used as the radial coordinate. Also computing time was greatly increased as the number of radial grid points increased; therefore, the number of grid points that could be used to demonstrate the effect of grid spacing was rather limited. As shown in Figure 3 few grid points resulted in very large point spacings near the centerline, which yielded excessively large values of $\partial\overline{Y}/\partial r$ and $\partial\overline{V}_z/\partial r$ (because of symmetry these terms always should equal zero at the centerline) and correspondingly small values of ξ in this region.

In Figure 3, the case designated "Interpolated" was obtained by selecting only five points from the computed profiles in Figures 1 and 2, and interpolating an additional 36 points using a second order interpolation routine, machine plotting the results to a large scale, and smoothing any interpolation errors by hand. Although only 41 grid points were used at each axial station in the interpolated case, their closer spacing near the centerline resulted in much better agreement with the input value of $\xi = 0.02$ (Figure 3) than did the 41 point case in which each grid point was exact (taken directly from Figures 1 and 2) but not closely spaced at the centerline. Unfortunately, because the case of the 100 grid points required excessive computing time for the numerical integration with which $\overline{Y}$, $\overline{V}_z$, and $\overline{\rho}$ profiles were computed, it was necessary to limit the axial distance over which these profiles were computed to only 1.5 in. rather than 15 in. as was obtained for the 21 and 41 grid points.

From Equations (27) to (30), it is obvious that values of the transport coefficients cannot be obtained <u>at</u> the centerline since both the integral terms as well as the radial derivatives are zero at this point. Of course, transport coefficients can be obtained as close to the centerline as desired as long as reliable data (or interpolations) are available. However, the coefficients could be evaluated at the centerline if the appropriate forms of Equations (20) to (23) are used. The symmetry conditions allow simplification of these equations at the centerline to give*,

<u>Centerline Diffusion Equation</u>

$$\overline{\rho V}_z \frac{\partial \overline{Y}}{\partial z} = 2\overline{\rho}(D + E_d) \frac{\partial^2 \overline{Y}}{\partial r^2} \tag{43}$$

<u>Centerline Radial Momentum Equation</u>

$$\overline{V}_r = 0 \tag{44}$$

<u>Centerline Axial Momentum Equation</u>

$$\overline{\rho V}_z \frac{\partial \overline{V}_z}{\partial z} = 2(\mu + \epsilon_3) \frac{\partial^2 \overline{V}_z}{\partial r^2} - g_c \frac{\partial \overline{P}}{\partial z} \tag{45}$$

<u>Centerline Energy Equation</u>

$$\begin{aligned}\overline{\rho V}_z \frac{\partial \overline{H}}{\partial z} &= 2\left(\frac{k}{C_p} + \overline{\rho}E_h\right) \frac{\partial^2 \overline{H}}{\partial r^2} + \\ &+ 2\sum_i \left[D\left(1 - \frac{1}{Le}\right) + E_d\left(1 - \frac{1}{Le_T}\right)\right] \overline{\rho}\overline{h}_i \frac{\partial^2 \overline{Y}_i}{\partial r^2} + \\ &+ \frac{1}{g_c}\left[\mu\left(1 - \frac{1}{Pr}\right) + \overline{\rho}E_m\left(1 - \frac{1}{Pr_T}\right)\right] \frac{\partial^2 \overline{V}_z^2}{\partial r^2}\end{aligned} \tag{46}$$

---

* If the function differentiated is symmetrical about the axis, $\lim_{r \to 0} \frac{1}{r} \frac{\partial}{\partial r}\left(\varphi r \frac{\partial}{\partial r}\right) = 2\varphi \frac{\partial^2}{\partial r^2}$.

Values of the transport coefficients at the centerline in principle can be obtained from these equations. Of course, extremely accurate closely-spaced experimental data (or interpoltations) would have to be available for the evaluation of second derivatives. The alternative of using Equations (27) to (30) to determine transport coefficients as close to the axis as possible and then extrapolating smooth continuous curve to the centerline (using the symmetry conditions) is very appealing since in this procedure the difficult problem of the evaluation of second derivatives is eliminated. Results obtained with the Interpolated case in Figure 3 show this later procedure yields reasonable results.

In the intermediate region between 0.2 to 1.5 in. in Figure 3, the value of the transport coefficients for all four curves had a maximum deviation from the correct value of only ±25%. This agreement is rather remarkable considering that for the case of 21 grid points only slightly more than a total of 80 input points were used at the four axial stations, each separated from the other by 5 in., and that in the interpolated case a total of only 20 original points was used, some of which were more than 0.5 in. from neighboring points of the profile. The oscillations that occur in the Interpolated case (Figure 3) primarily were caused by the difficulty in differentiating interpolated data, and the discrepancies in the hydrogen mass balances which resulted in inaccuracies in $\partial\bar{Y}/\partial r$ and in the axial derivatives of the integral in Equation (27). However, these results clearly demonstrate that very reasonable approximations of transport coefficients may be obtained from rather limited experimental data.

Figures 3 and 4 show that at radial positions greater than 1.5 in. at which $\overline{Y}$ approachs zero (Figure 1) valid coefficients cannot be obtained. In this region, both the axial derivative of the integral in Equation (27) and $\partial\overline{Y}/\partial r$ approach zero as the free stream is approached, so that their ratio cannot be accurately determined. As $r \rightarrow \infty$ and each of these terms becomes zero, the computer designates 0/0 as 0.

Figure 4 illustrates the effect of axial station on ξ for the 41 point grid. Best results are obtained at intermediate axial stations rather than at the end points; of course, this result would be expected because of the difficulty in obtaining accurate slopes from polynomial fits at end points. However, very reasonable agreement was obtained between the computed and input values of ξ at the intermediate axial stations for this case.

The general conclusions to be obtained from this test case is that approximate values of the turbulent transport coefficients can be obtained from a limited number of experimental data points, as long as the original points are reasonably accurate. However, since point spacing is important even when the data points are exact, some ambiguity of results is to be expected when using experimental profiles. That is, reasonably closely spaced accurate experimental data must be used in order to obtain detailed variations of the transport coefficients.

VI. REFERENCES

1. Schlichting, H., Boundary Layer Theory, 1st ed. McGraw-Hill, New York (1962) Chapter XIX, p. 502.

2. Vasiliu, J., J. Aerospace Sci., 29, 19 (1962).

3. Libby, P.A., ARS J., 32, 388 (1962).

4. Kleinstein, G., J. Spacecraft Rockets, 1, 403 (1964).

5. Ferri, A., J. Roy. Aeronautical Soc., 68, 575 (1964).

6. Pai, S.I., Quar. Appl. Math., 10, 141 (1952).

7. Zeiberg, S.L., and Bleich, G.D., "A Finite-Difference Method Solution of the Laminar Hypersonic, Non-Equilibrium Wake", GASL TR-338, February 1963.

8. Zakkay, V., Krause, E., and Woo, S.D.L., AIAA J., 11, 1939 (1964); raw data presented in "Turbulent Transport Properties for Axisymmetric Heterogeneous Mixing", Polytechnic Institute of Brooklyn, Report No. 813, March 1964.

9. Zakkay, V., and Krause, E., Int. J. Heat Mass Transfer, 8, 1047, (1965).

10. Morgenthaler, J.H., "Supersonic Mixing of Hydrogen and Air", Ph.D. Thesis, University of Maryland (1965).

11. Morgenthaler, J.H., and Marchello, J.M., "Turbulent Transport Coefficients in Supersonic Flow", Paper 34d presented at Symposium on Fundamentals and Fluid Dynamics, AIChE Philadelphia Meeting, December 1965, Accepted for Publication in Int. J. Heat Mass Transfer.

12. Hinze, J.O., Turbulence , McGraw-Hill, New York (1959), p. 407, 416.

13. Lanczos, C., Applied Analysis, Prentice Hall, Englewood Cliff, N. J., (1956) pp. 321-324.

14. Pai, S.I., Viscous Flow Theory II - Turbulent Flow, Van Nostrand, Princeton, N.J., (1957), Chapters I, VIII.

15. Hinze, J.O., _Turbulence_, McGraw-Hill, New York (1959) Chapter 5.

16. Van Driest, E.R., _J. Aeronautical Sciences,_ 18, 145 (1951).

17. Levenspiel, O., _Chemical Reaction Engineering_, Wiley, N.Y. (1962), p. 262.

18. Alpinieri, L.J., _AIAA J._, _2_, 1560 (1964).

19. Page, F., Schlinger, W.G., Breaux, D.K., and Sage, B.H., _Ind. Eng. Chem._, _44_, 424 (1952).

APPENDIX A

EXPERIMENTALLY DETERMINED TURBULENT TRANSPORT COEFFICIENTS

One objective of the present investigation was to use the numerical technique presented herein to determine turbulent transport coefficients for the case of supersonic, coaxial, free-jet mixing. Unfortunately, no completely adequate (closely-spaced) experimental data were available for this purpose. However, experimental data presented in Reference 8, which generally contained five or six radial experimental data points at each of six axial station could be used if addition points were generated by interpolation as had been done in the Interpolated test case previously discussed. Of course, in the present case the experimental data points were not necessarily exact, as they had been in the test case (where the points were computed); therefore, any errors in the original points were transmitted to the interpolated points, so that discrepancies in the original points were magnified when the resulting profiles were differentiated. Clearly, detailed variation of turbulent transport coefficients only can be obtained from closely-spaced, accurate data points.

The data of Reference 8 obtained for the case of coaxial, free-jet mixing of subsonic hydrogen (M=0.5 to 0.9) with a surrounding Mach 1.6 air jet (1.1 lb/sec) at an overall equivalence ratio (ER) of 0.10 to 0.25. Stagnation temperature and static pressure were assumed constant throughout the mixing region in the computation of velocities and densities as had been done in Reference 8. Typical concentration and velocity profiles obtained at six axial stations between 4 and 9 in. downstream of the injection station are presented in Figures 5 and 6 for a hydrogen mass flow rate of approximately 0.007 lb/sec (M=0.89) into a 1.1 lb/sec, Mach 1.6 air stream (ER = 0.25). Original data points are plotted as symbols in these figures; the final interpolated (and somewhat smoothed) profiles used to determine the turbulent transport coefficients are plotted as solid lines.* Conditions for this run, designated Case C, are summarized in Table 1, along with runs A and B. The mass and momentum balances computed at each axial station are presented in Table 2. A sufficient number of points were interpolated for each of the experimental profiles, so that a total of more than 40 points were available at each axial station. Grid spacing at the centerline was approximately 0.017 in. and at the free stream 0.020 in.

The turbulent mass transfer coefficient, ξ, as well as the eddy diffusivity of mass, E_d, ($\xi \equiv \bar{\rho} E_d$) and the eddy diffusivity of momentum, E_m were obtained using Equations (27) and (28), and the procedure previously discussed. Typical results, obtained for Case C, are presented in Table 3. As anticipated considerable variation occurred in these transport coefficients because of the inconsistencies in the mass balances and the difficulties inherent in differentiating interpolated experimental data starting with only a few original data points. In addition, some error may have been introduced in the velocity profiles by the assumption that the local free stream static pressure and the stagnation temperature were constant throughout the mixing region. Because of these problems, better values of E_m were obtained by assuming $Sc_T = 1$ than by direct differentiation of the velocity profiles. Therefore, experimental values of E_m and Sc_T are not reported. Despite the variation that occurred in the derived transport coefficients, certain trends appeared, which generally were consistent for each of the cases analyzed.

---

* For the purpose of the initial computations, the axial symmetry indicated by the dashed lines in Figures 5 to 8 was not considered; rather the best smooth curves through the experiental data were used.

As a first approximation, a model was constructed simplifying the major trends shown in Table 3 to include only radial dependence of ξ and E_d. In order to determine whether or not these trends were at least a valid first approximation, the program for the numerical integration of the diffusion, momentum, and energy equations[7] was used to compute $\bar{Y}$, $\bar{V}_z$, and $\bar{\rho}$ profiles at various downstream locations using the simplified trends as input to the program. This test was similar to those previously reported[10], except for two important differences: 1). In the present numerical integration technique, the stream function, ψ, was used as the radial coordinate. Because of this transformation the radial velocity, $\bar{V}_r$, did not have to be specified in advance as was previously required; only E_d needed to be specified when the assumption was made that $Sc_T = Le_T = Pr_T = 1$. Therefore, the agreement obtained between computed and experimental profiles was a direct evaluation of the validity of the particular model being tested. 2). A variable radial grid spacing in physical coordinates was used in Reference 10 which significantly reduced the number of radial grid points required, thereby greatly shortening computing time. Results are presented for all trials and all cases in Tables 4 to 12 and for the best results with Case C in Figures 7 and 8; agreement between experimental and computed concentration and velocity profiles is reasonably good for the last trial in each case, as shown in Tables 5,6,8,9, 11, and 12. The transport coefficients used in these numerical integrations are tabulated in Tables 4,7, and 10; linearly interpolated values were used at radial positions intermediate to those tabulated. Comparison of the various cases shows that a relatively small change in E_d or ξ results in a rather large change in computed concentration profiles, but not nearly as significant a change in the computed velocity profiles. Also, reasonable agreement was attained using the simple trends. Additional computer trials must be made in order to determine whether E_d and ξ is more basic for correlation of data. Further evidence concerning this important point could be obtained in future work by analyzing the argon and helium mixing data also available in Reference 8.

Because an insufficient number of data points were available to accurately define radial profiles, especially at the centerline where symmetry required that $\partial\bar{Y}/\partial r$ and $\partial\bar{V}_z/\partial r=0$ (see Figures 5 and 6), cosine profiles of the form

$$\bar{Y} = Y_o + A \cos (\alpha r) \tag{A-1}$$

$$\bar{V}_z = V_{z_o} + B \cos (\beta r) \tag{A-2}$$

were fitted through experimental points located at radial positions of 0, 0.125, and 0.25 in. These cosine fits were more general than those used in Reference 8, in which two rather than three arbitrary constants were used. As shown in Tables 13 and 14 considerable smoothing of both E_d and ξ occurred using these fits; however, overall results were not drastically changed from those obtained with the smoothed data, except that values near the centerline were increased because the curvature of the cosine is maximum at the origin.

The good agreement between computed and experimental $\bar{Y}$ and $\bar{V}_z$ profiles shown in Figures 7 and 8 and in Tables 5,6,8,9,11, and 12, obtained using the simplified trends, substantiate the validity of these trends and suggest that for these data radial variation of the transport coefficients is more signicant than axial variation, and E_d reaches a maximum at about 20% of the distance from the centerline to the free stream. Similar trends were reported in Reference 19 for subsonic flow between two parallel plates. Further invesitgation is required to confirm these important points.

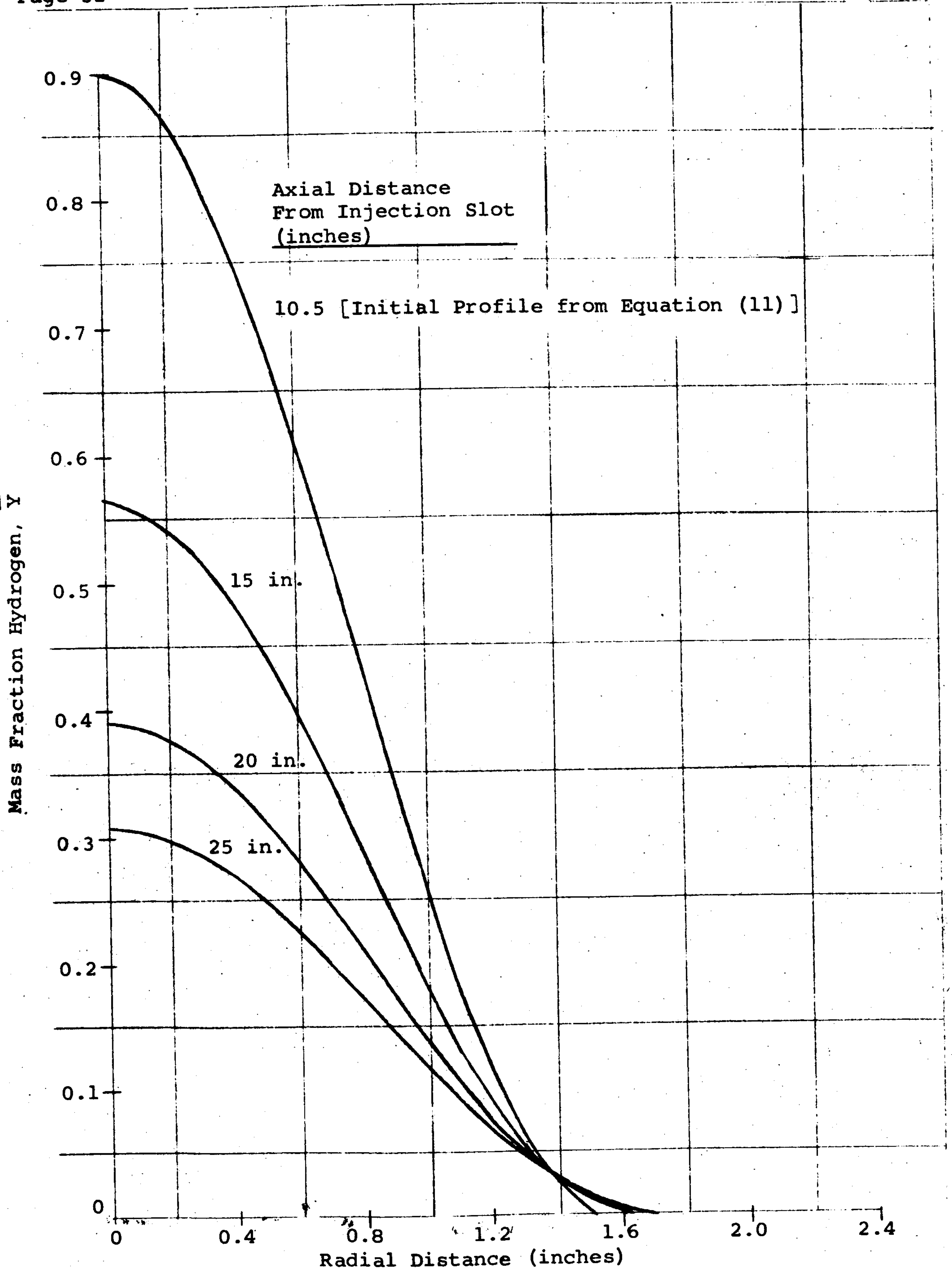

FIGURE 1 - COMPUTED HYDROGEN CONCENTRATION PROFILES, TEST CASE

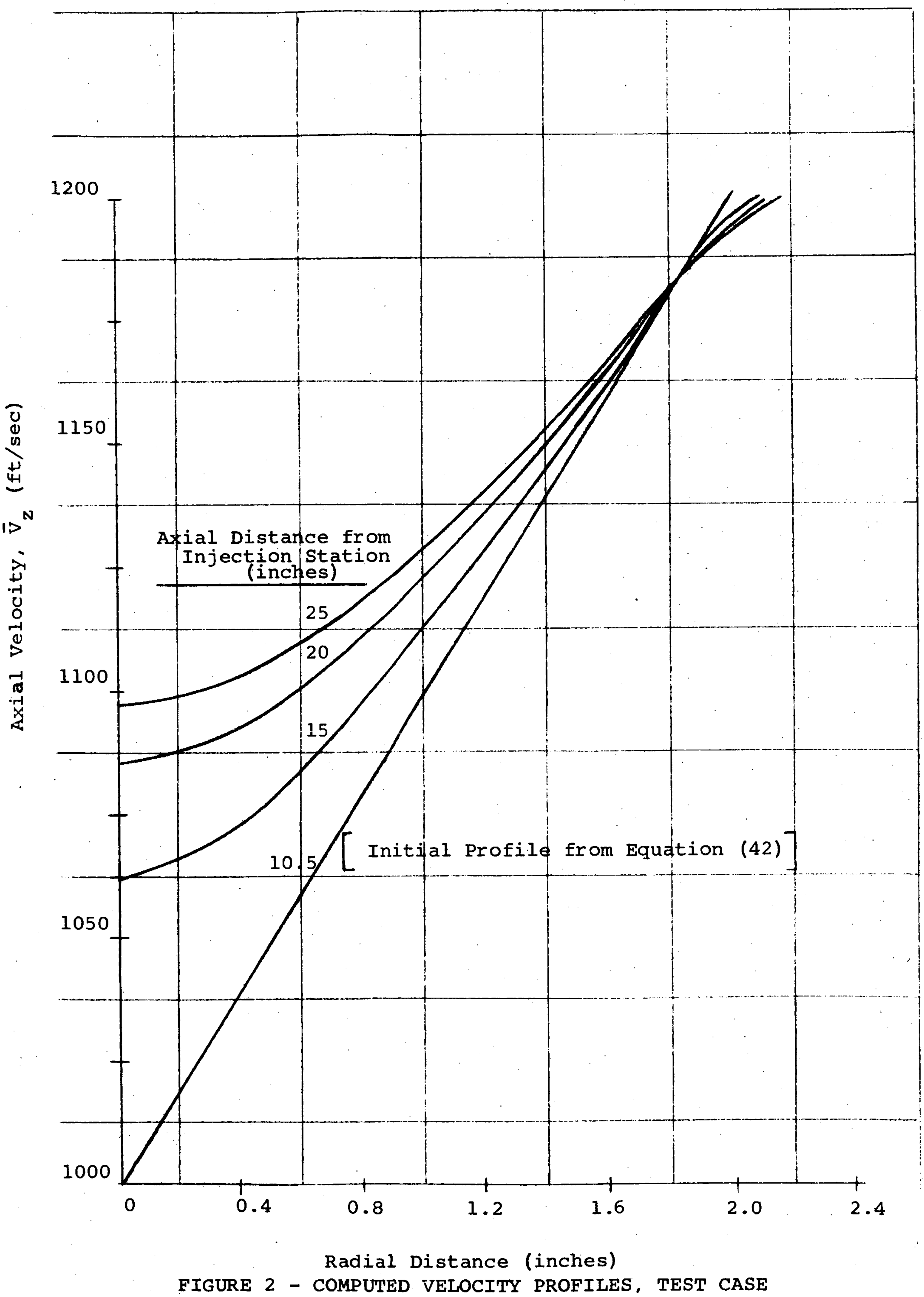

FIGURE 2 - COMPUTED VELOCITY PROFILES, TEST CASE

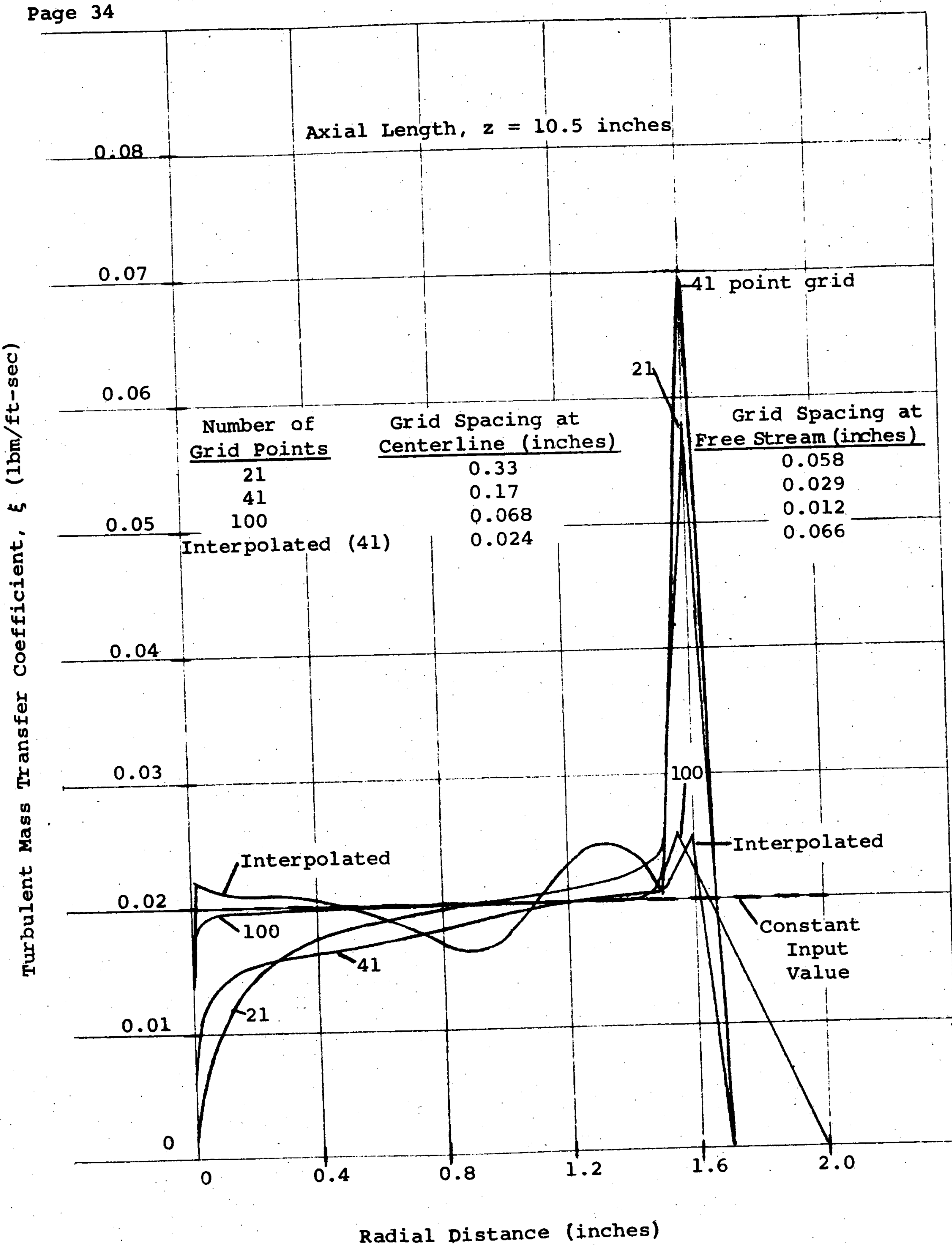

FIGURE 3 - EFFECT OF RADIAL GRID SPACING ON ξ, TEST CASE

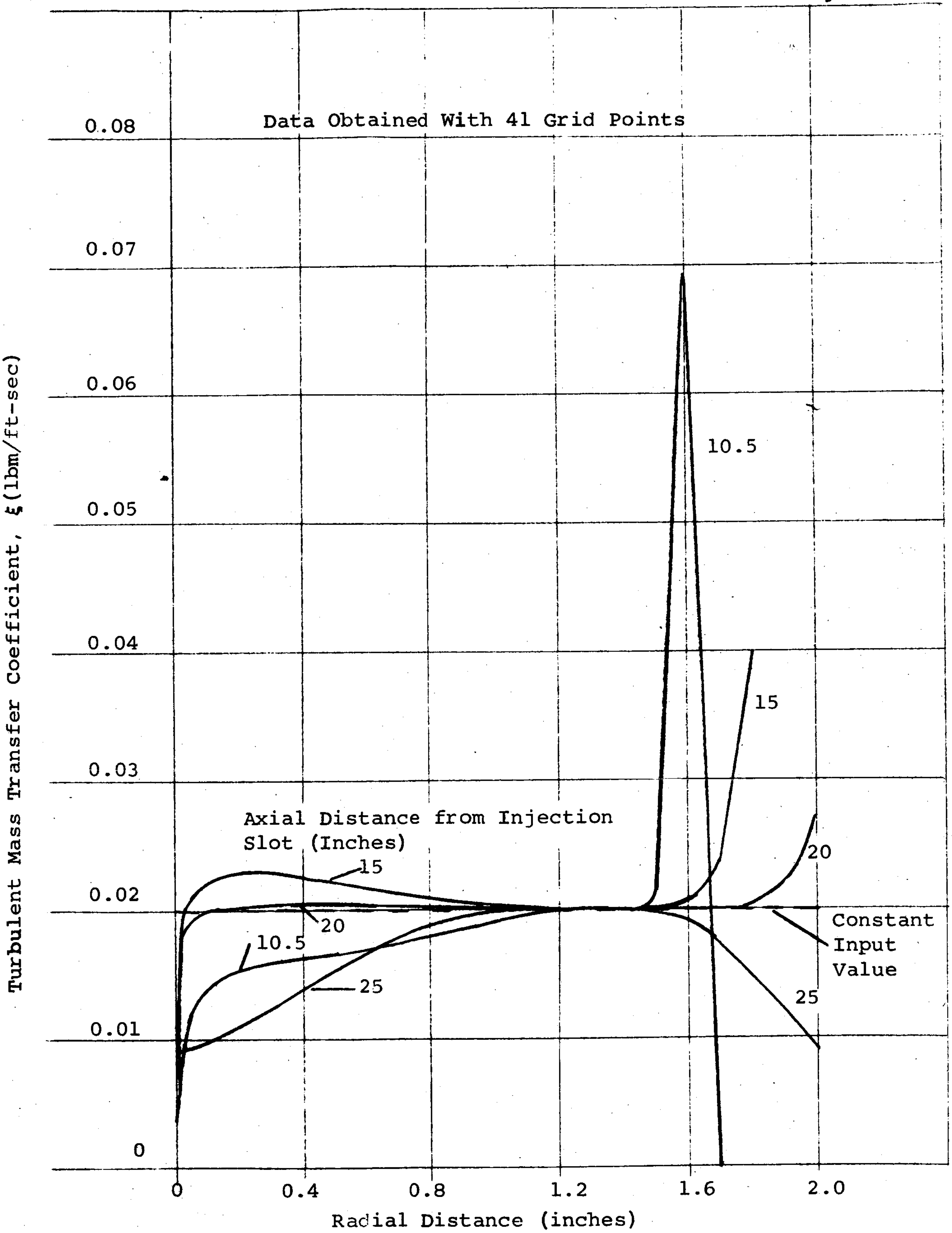

FIGURE 4 - EFFECT OF AXIAL POSITION ON ξ, TEST CASE

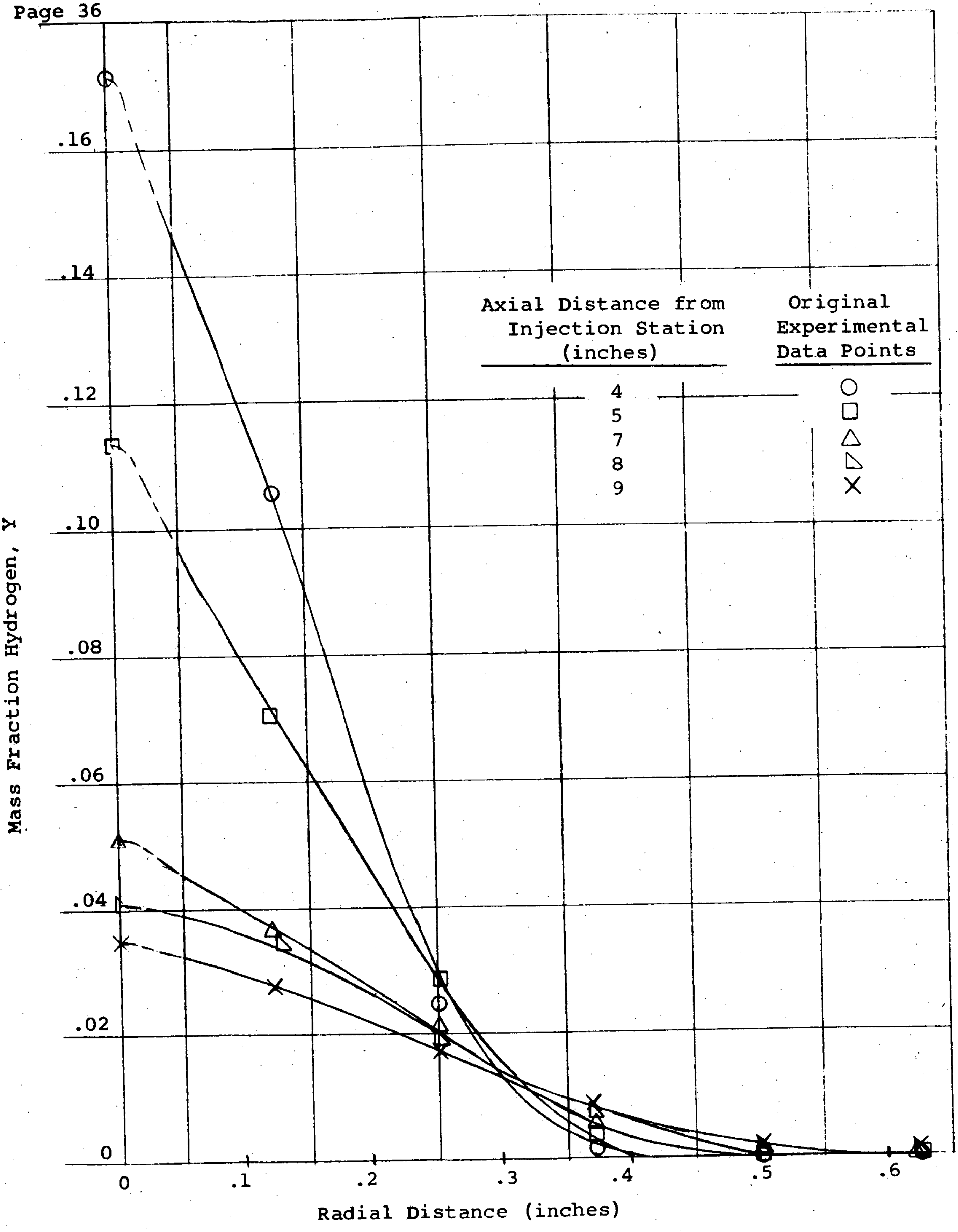

FIGURE 5 - EXPERIMENTAL CONCENTRATION PROFILES, CASE C

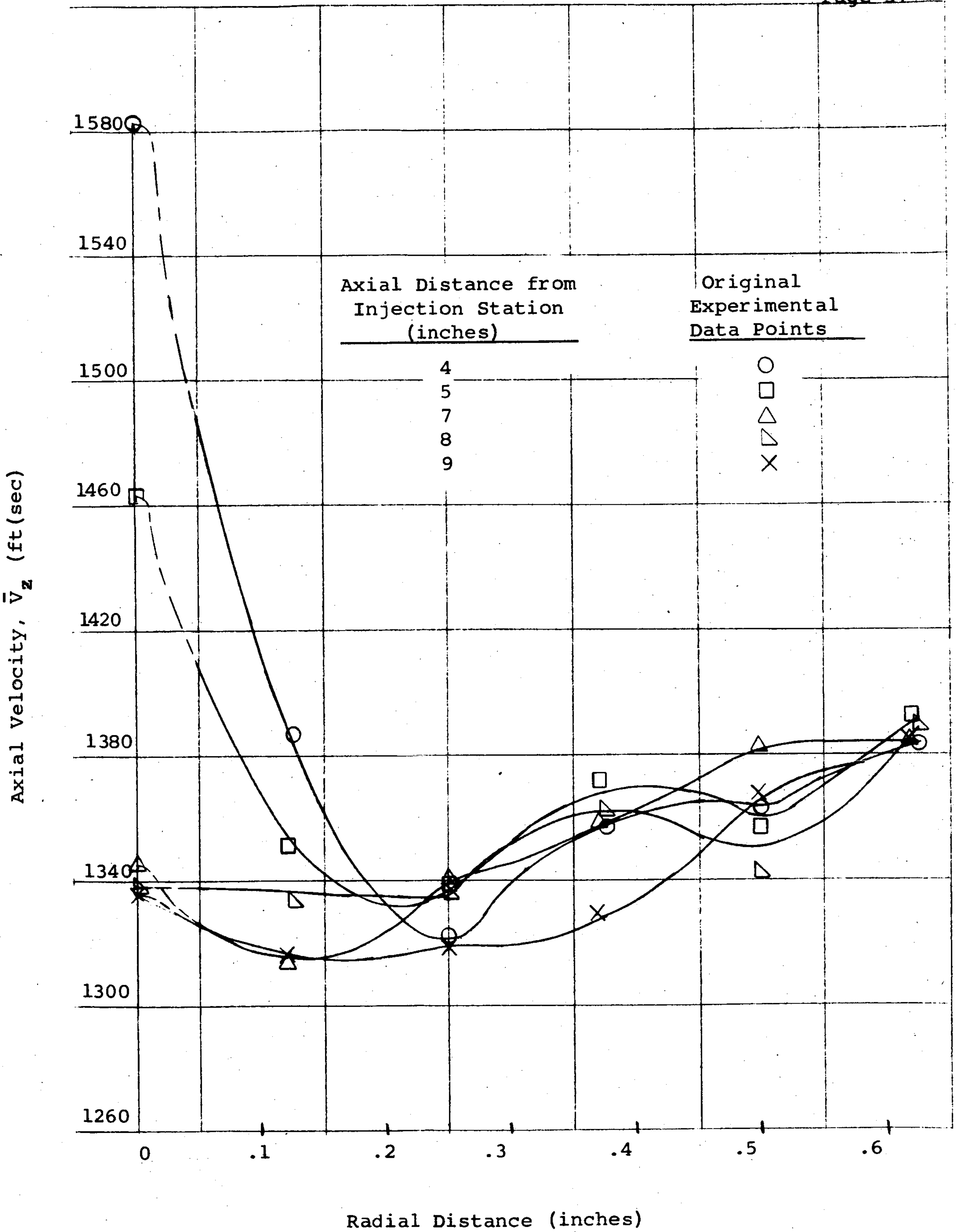

FIGURE 6 - EXPERIMENTAL VELOCITY PROFILES, CASE C

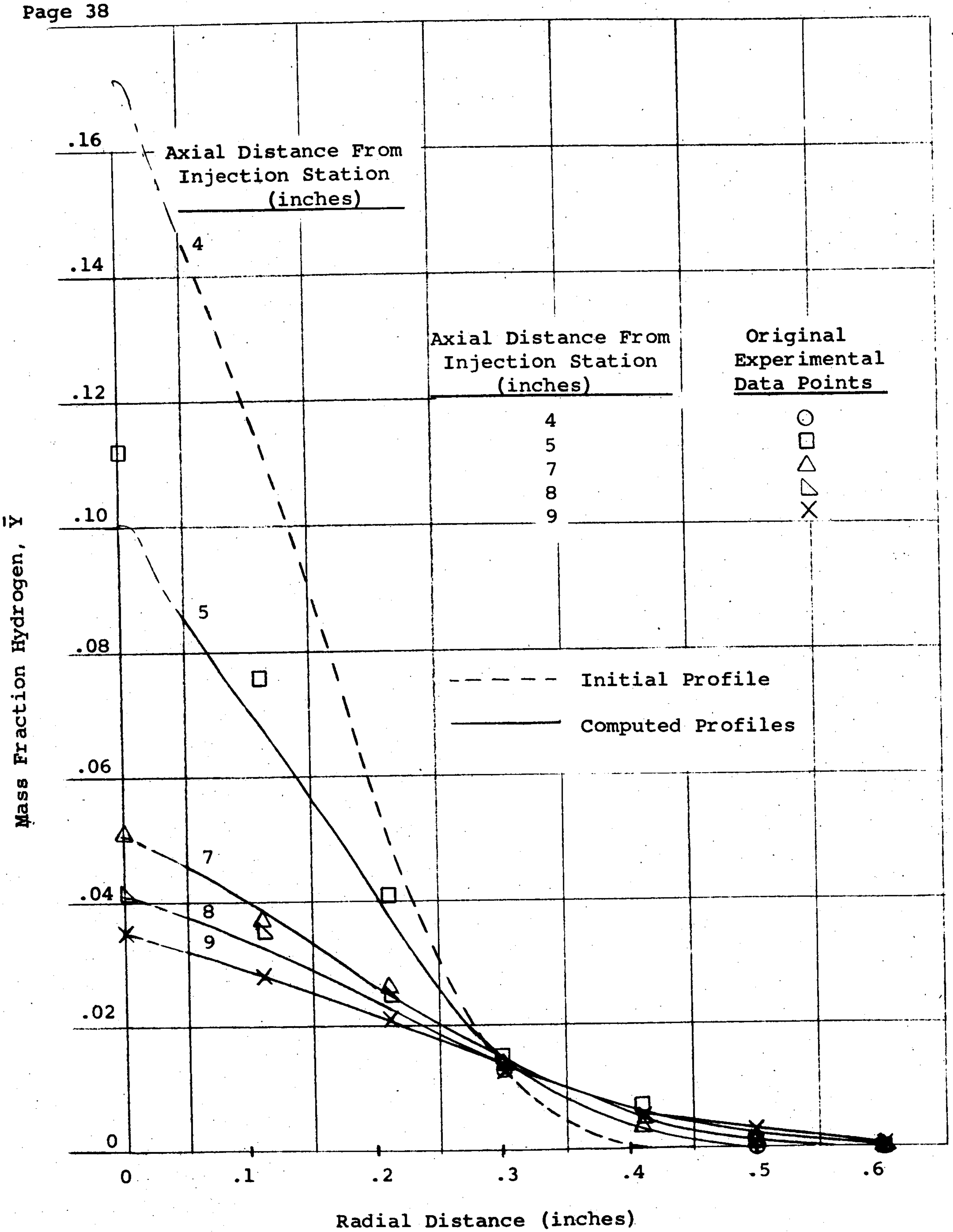

FIGURE 7 - COMPARISON OF COMPUTED CONCENTRATION PROFILES WITH EXPERIMENTAL DATA

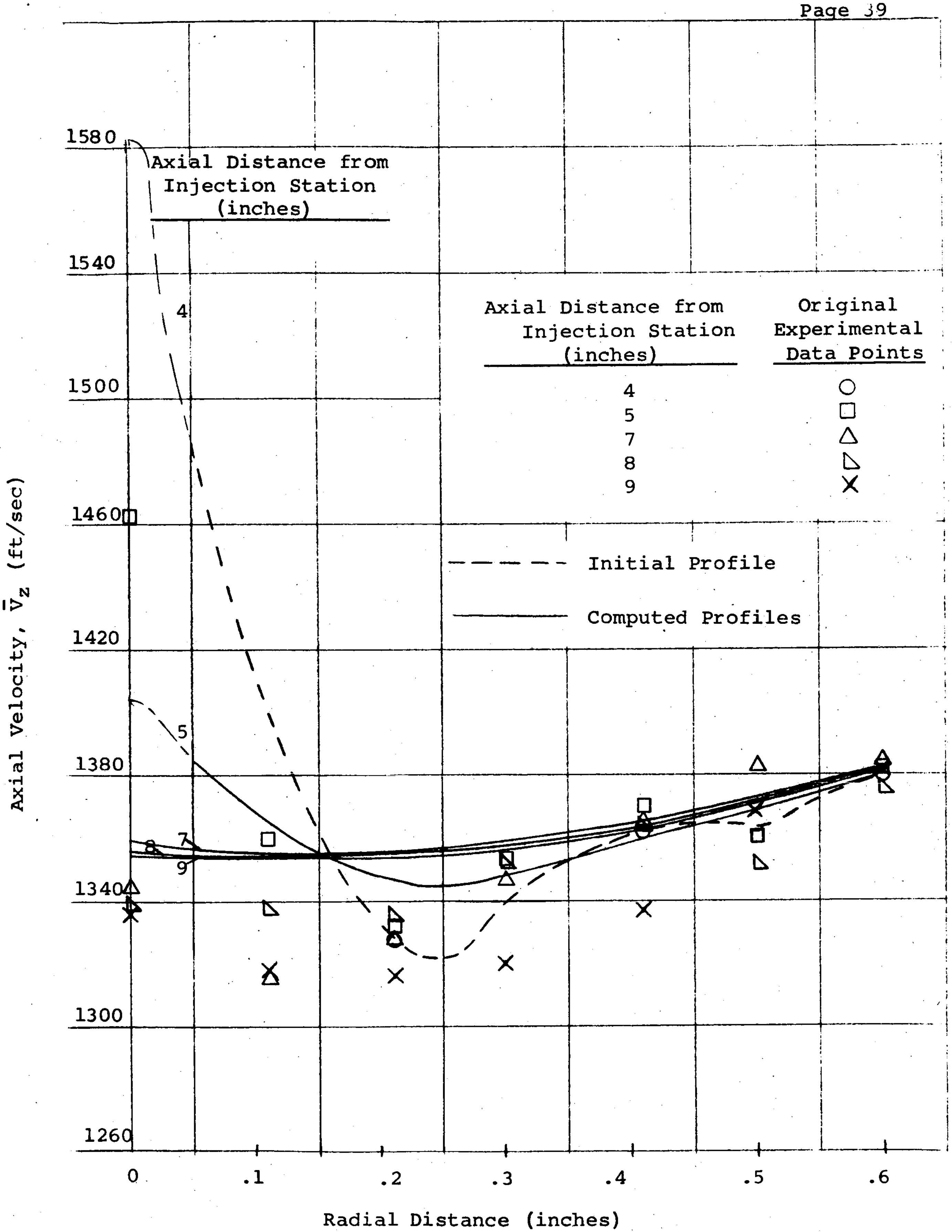

FIGURE 8 - COMPARISON OF COMPUTED VELOCITY PROFILES WITH EXPERIMENTAL DATA

TABLE 1

TEST CONDITIONS FOR THE HYDROGEN-AIR COAXIAL, MIXING EXPERIMENTS OF REFERENCE 8

Test section wall static pressure (assumed constant throughout flow)	13.0 psia
Stagnation temperature (assumed constant throughout flow)	$520^{o}R$
Diameter hydrogen jet	0.3 inches
Diameter external air stream	3.44 inches
Diameter of mixing section	12 inches
Mach number external air stream	1.6
Air mass flow rate	1.1 lb/sec.

CASE	A	B	C
Mach number hydrogen jet	0.51	0.60	0.89
$\rho_j V_j / \rho_e V_e$	0.047	0.072	0.125
V_j / V_e	1.455	1.690	2.42
Hydrogen mass flow rate (lb/sec)	0.003	0.004	0.007
Overall Equivalence ratio	0.10	0.13	0.25

TABLE 2

MASS AND MOMENTUM BALANCE FOR HYDROGEN-AIR, COAXIAL, MIXING EXPERIMENTS OF REF. 8

CASE	AXIAL LENGTH (in.)	$\sum_i (\rho V_z YA)_i$ lb H_2/sec.	$\sum_i (\rho V_z A)_i$ lb H_2+Air/sec	$\sum_i (\frac{\rho}{g_i} V_z^2 A)_i$ lbf
A	3	0.0043	1.063	44.79
	5	0.0028	1.107	46.07
	6	0.0027	1.133	47.60
	7	0.0022	1.121	46.58
	8	0.0022	1.112	45.90
	9	0.0022	1.124	46.86
B	4	0.0045	1.081	45.30
	5	0.0041	1.074	44.50
	6	0.0046	1.118	47.54
	7	0.0034	0.993	39.08
	8	0.0041	1.108	46.62
	9	0.0037	1.020	40.82
C	4	0.0073	1.071	45.45
	5	0.0070	1.079	45.90
	7	0.0059	1.098	46.71
	8	0.0066	1.074	45.43
	9	0.0064	1.067	44.91

TABLE 3

TURBULENT TRANSPORT COEFFICIENTS, CASE C

Z(in.) / R(in.)	E_d (ft^2/sec)					ξ (lbm/ft-sec)				
	4.0	5.0	7.0	8.0	9.0	4.0	5.0	7.0	8.0	9.0
.006	0.0751	0.0531	0.0542	0.1443	0.0466	0.0018	0.0017	0.0026	0.0077	0.0027
.013	0.1393	0.1015	0.1041	0.2441	0.0859	0.0033	0.0032	0.0051	0.0131	0.0049
.026	0.2582	0.1913	0.1941	0.3703	0.1527	0.0064	0.0062	0.0096	0.0200	0.0088
.039	0.3589	0.2727	0.2727	0.4432	0.2062	0.0091	0.0091	0.0137	0.0240	0.0120
.052	0.4421	0.3444	0.3405	0.4843	0.2496	0.0115	0.0118	0.0174	0.0264	0.0146
.104	0.6219	0.5345	0.5177	0.5109	0.3602	0.0187	0.0207	0.0280	0.0289	0.0219
.156	0.6056	0.5781	0.5764	0.4688	0.4282	0.0220	0.0257	0.0334	0.0279	0.0272
.208	0.4475	0.4906	0.5482	0.4092	0.4726	0.0211	0.0258	0.0345	0.0263	0.0317
.260	0.4032	0.3875	0.4267	0.4200	0.4766	0.0265	0.0249	0.0298	0.0297	0.0342
.312	0.4238	0.3296	0.3715	0.4337	0.4576	0.0336	0.0254	0.0289	0.0333	0.0349
.351	0.3855	0.3160	0.3477	0.3829	0.4064	0.0342	0.0272	0.0291	0.0311	0.0325
.403	0.8598	0.5016	0.3383	0.2867	0.2991	0.0814	0.0474	0.0305	0.0248	0.0253
.455	0	2.6733	0.2954	0.1826	0.1720	0	0.2566	0.0280	0.0165	0.0153
.507	0	0	0.7428	0.1148	0.0732	0	0	0.0719	0.0107	0.0068
.559	0	0	0	0.0368	-0.0617	0	0	0	0.0035	-0.0058
.611	0	0	0	-0.6539	-0.3042	0	0	0	-0.0634	-0.0294
.650	0	0	0	0.344	0.1606	0	0	0	0.0338	0.0157

TABLE 4

TURBULENT TRANSPORT COEFFICIENTS USED IN NUMERICAL INTEGRATION, CASE A*

	TRIAL					
	1	2	3	4	5	6
R inches	ρE_d lbm/ft-sec	ρE_d lbm/ft-sec	ρE_d lbm/ft-sec	ρE_d lbm/ft-sec	E_d ft^2/sec	E_d ft^2/sec
0	0.02	.0025	.0025	.0025	.025	.050
.05	- **	.0325	.0175	.0325	.475	.500
.10	-	.0475	.0250	.0550	.680	.750
.15	-	-	-	-	.800	.900
.20	-	.0500	.0300	.0750	-	-
.225	-	-	-	-	.630	-
.30	-	-	-	-	.675	-
.35	-	-	-	-	.575	-
.40	-	-	-	-	.600	-
.425	-	-	-	-	.550	-
.50	-	-	-	-	.450	.500
.60	-	-	-	.0350	-	-
.70	0.02	.0500	.0300	.0350	1.000	.500

* In all trials the assumption was made that $E_d = E_m$, i.e., $Sc_T = 1$.

** Linear interpolation was used for evaluation of coefficients at radial positions intermediate to tabulated values.

TABLE 5

COMPARISON BETWEEN EXPERIMENTAL AND COMPUTED CONCENTRATION PROFILES, CASE A

HYDROGEN CONCENTRATION

R (in.)	z = 3" Initial Exper. Profile	z = 5" Exper.	z = 5" TRIAL 1	2	3	4	5	6	z = 6" Exper.	z = 6" TRIAL 1	2	3	4	5	6
0	0.071	.026	.037	.029	.037	.025	.041	.029	.015	.031	.021	.029	.018	.028	.019
0.11	0.063	.021	.031	.020	.027	.017	.021	.019	.015	.026	.016	.021	.013	.017	.014
0.21	0.039	.013	.021	.015	.018	.013	.015	.014	.010	.018	.012	.015	.010	.012	.011
0.30	0.015	.006	.010	.009	.010	.009	.009	.008	.005	.010	.008	.009	.008	.008	.008
0.41	0	.0004	.002	.003	.003	.004	.003	.003	.0009	.003	.004	.003	.004	.004	.004
0.50	0	0	.0002	.001	.0005	.001	.001	.001	.0003	.0004	.002	.001	.002	.001	.002
0.60	0	0	0	.0001	0	.0002	.0001	.0002	.00007	0	.0004	0	.0005	.0003	.0005

R (in.)	z = 7" Exper.	z = 7" TRIAL 1	2	3	4	5	6	z = 9" Exper.	z = 9" TRIAL 1	2	3	4	5	6
0	.012	.025	.016	.023	.014	.020	.014	.008	.020	.012	.017	.010	.012	.010
0.11	.010	.022	.013	.018	.011	.014	.012	.007	.018	.010	.014	.008	.010	.009
0.21	.007	.015	.010	.013	.009	.010	.009	.006	.014	.008	.011	.007	.008	.007
0.30	.004	.009	.007	.008	.007	.007	.007	.004	.008	.006	.008	.006	.006	.006
0.41	.001	.003	.004	.003	.004	.004	.004	.002	.003	.004	.004	.004	.004	.004
0.50	.0007	.001	.002	.001	.002	.002	.002	.0009	.001	.002	.002	.003	.002	.002
0.60	0	.0001	.0007	.0002	.0007	.004	.0006	.0002	.0002	.001	.0005	.001	.0006	.001

TABLE 6

COMPARISON BETWEEN EXPERIMENTAL AND COMPUTED VELOCITY PROFILES, CASE A

VELOCITY (ft/sec)

R (in.)	z = 3" Initial Exper. Profile	z = 5" Exper.	z = 5" TRIAL 1	2	3	4	5	6	z = 6" Exper.	z = 6" TRIAL 1	2	3	4	5	6
0	651	1161	1004	1086	997	1127	956	1086	1269	1078	1174	1092	1209	1097	1193
.11	702	1186	1055	1177	1110	1212	1162	1191	1282	1118	1225	1165	1256	1218	1242
.21	972	1255	1176	1240	1208	1260	1240	1250	1308	1210	1270	1235	1285	1266	1277
.30	1240	1311	1295	1303	1293	1305	1305	1305	1337	1295	1313	1303	1314	1313	1314
.41	1394	1335	1375	1363	1368	1356	1362	1360	1352	1369	1359	1364	1353	1358	1357
.50	1401	1356	1397	1388	1393	1385	1388	1386	1368	1392	1382	1389	1378	1384	1380
.60	1401	1356	1400	1399	1400	1399	1400	1399	1369	1400	1396	1400	1395	1397	1395

R (in.)	z = 7" Exper.	z = 7" TRIAL 1	2	3	4	5	6	z = 9" Exper.	z = 9" TRIAL 1	2	3	4	5	6
0	1230	1127	1224	1151	1252	1184	1246	1279	1183	1274	1213	1295	1265	1293
.11	1243	1160	1258	1203	1282	1253	1274	1286	1205	1293	1246	1310	1292	1306
.21	1279	1230	1290	1260	1301	1285	1296	1299	1256	1313	1282	1321	1310	1319
.30	1310	1302	1320	1310	1322	1321	1324	1318	1310	1333	1317	1335	1332	1334
.41	1333	1365	1357	1360	1353	1357	1355	1336	1361	1359	1358	1355	1359	1357
.50	1353	1390	1378	1385	1374	1381	1378	1352	1385	1376	1380	1372	1379	1374
.60	1368	1400	1393	1398	1392	1395	1393	1363	1398	1389	1394	1387	1393	1389

TABLE 7

TURBULENT TRANSPORT COEFFICIENTS USED IN NUMERICAL INTEGRATION, CASE B*

R inches	TRIAL 1 ρE_d lbm/ft-sec	TRIAL 2 ρE_d lbm/ft-sec	TRIAL 3 ρE_d lbm/ft-sec
0	0.02	0.01	0.010
.020	-**	-	0.010
.026	-	-	0.012
.035	-	-	0.015
.065	-	-	0.015
.085	-	-	0.020
.100	-	-	0.030
.700	0.02	0.01	0.030

* In all trials the assumption was made that $E_d = E_m$, i.e., $Sc_T = 1$

** Linear interpolations was used for evaluation of coefficients at radial positions intermediate to tabulated values.

TABLE 8

COMPARISON BETWEEN EXPERIMENTAL AND COMPUTED CONCENTRATION PROFILES, CASE B

HYDROGEN CONCENTRATION

R (in.)	z = 4" Initial Exper. Profile	z = 5" Exper.	z = 5" Trial 1	z = 5" Trial 2	z = 5" Trial 3	z = 6" Exper.	z = 6" Trial 1	z = 6" Trial 2	z = 6" Trial 3	z = 7" Exper.	z = 7" Trial 1	z = 7" Trial 2	z = 7" Trial 3
0	0.099	.058	.053	.065	.050	.037	.039	.052	.035	.029	.032	.045	.027
0.11	0.061	.041	.042	.050	.036	.032	.033	.042	.027	.023	.027	.037	.022
0.21	0.028	.021	.024	.024	.021	.020	.020	.023	.017	.015	.018	.021	.015
0.30	0.008	.008	.008	.009	.009	.009	.009	.008	.009	.007	.009	.009	.009
0.41	0.0003	.003	.001	.0008	.002	.002	.002	.001	.003	.001	.003	.002	.003
0.50	0	0	0	0	.0002	0	.0003	0	.0006	0	.0006	.0002	.001
0.60	0	0	0	0	0	0	0	0	0	0	0	0	.0001

R (in.)	z = 8" Exper.	z = 8" Trial 1	z = 8" Trial 2	z = 8" Trial 3	z = 9" Exper.	z = 9" Trial 1	z = 9" Trial 2	z = 9" Trial 3
0	.021	.027	.039	.022	.018	.024	.035	NOT AVAILABLE
0.11	.019	.024	.033	.019	.015	.021	.030	
0.21	.013	.016	.020	.013	.012	.015	.019	
0.30	.008	.009	.009	.008	.008	.009	.009	
0.41	.003	.003	.002	.003	.003	.003	.002	
0.50	.001	.0009	.0003	.001	.001	.001	.0005	
0.60	.0003	0	0	.0002	.0001	0	0	

TABLE 9

COMPARISON BETWEEN EXPERIMENTAL AND COMPUTED VELOCITY PROFILES, CASE B

VELOCITY (ft/sec)

R (in.)	z = 4" Initial Exper. Profile	z = 5" Exper.	z = 5" TRIAL 1	z = 5" TRIAL 2	z = 5" TRIAL 3	z = 6" Exper.	z = 6" TRIAL 1	z = 6" TRIAL 2	z = 6" TRIAL 3	z = 7" Exper.	z = 7" TRIAL 1	z = 7" TRIAL 2	z = 7" TRIAL 3
0	1000	1086	1106	1053	1122	1212	1173	1106	1197	1233	1212	1145	1236
.11	1044	1157	1158	1116	1189	1226	1207	1159	1236	1233	1236	1188	1262
.21	1237	1260	1260	1252	1270	1289	1275	1262	1285	1233	1285	1272	1296
.30	1342	1316	1330	1335	1330	1345	1327	1333	1326	1233	1327	1330	1327
.41	1361	1335	1360	1361	1359	1381	1358	1360	1355	1240	1355	1359	1353
.50	1365	1348	1365	1366	1366	1383	1365	1366	1365	1258	1365	1366	1363
.60	1370	1362	1370	1370	1370	1386	1370	1370	1370	1307	1370	1370	1370

R (in.)	z = 8" Exper.	z = 8" TRIAL 1	z = 8" TRIAL 2	z = 8" TRIAL 3	z = 9" Exper.	z = 9" TRIAL 1	z = 9" TRIAL 2	z = 9" TRIAL 3
0	1249	1237	1174	1260	1267	1254	1194	NOT AVAILABLE
.11	1267	1255	1208	1279	1267	1268	1222	
.21	1310	1292	1275	1304	1267	1298	1280	
.30	1340	1327	1327	1329	1267	1327	1327	
.41	1356	1354	1358	1351	1267	1352	1357	
.50	1361	1364	1365	1362	1274	1363	1365	
.60	1374	1370	1370	1370	1320	1370	1370	

TABLE 10

TURBULENT TRANSPORT COEFFICIENTS USED IN NUMERICAL INTEGRATION, CASE C*

	TRIAL		
	1	2	3
R inches	ρE_d lbm/ft-sec	E_d ft^2/sec	ρE_d lbm/ft-sec
0	0.02	0.050	0.0025
0.05	- **	-	0.0175
0.10	-	-	0.0250
0.20	-	-	0.0300
0.10	-	-	-
0.50	-	-	-
0.70	0.02	0.055	0.0300

* In all trials the assumption was made that $E_d = E_m$, i.e., $Sc_T = 1$.

** Linear interpolation was used for evaluation of coefficients at radial positions intermediate to tabulated values.

TABLE 11

COMPARISON BETWEEN EXPERIMENTAL AND COMPUTED CONCENTRATION PROFILES, CASE C

CONCENTRATION

R (in.)	z = 4" Exper.	z = 5" Exper.	z = 5" TRIAL 1	2	3	z = 7" Exper.	z = 7" TRIAL 1	2	3
0	0.170	.114	.098	.154	.101	.051	.057	.138	.051
.11	0.114	.076	.080	.110	.068	.037	.048	.097	.039
.21	0.050	.041	.041	.047	.038	.026	.031	044	.025
.30	0.013	.015	.014	.013	.015	.014	.015	.013	.015
.41	0.0003	.007	.002	.0006	.003	.003	.004	.001	.005
.50	0	0	.0001	0	.0002	.0001	.001	.0001	.002
.60	0	0	0	0	0	0	.0001	0	.0002

R (in.)		z = 8" Exper.	z = 8" TRIAL 1	2	3	z = 9" Exper.	z = 9" TRIAL 1	2	3
0		.041	.048	.131	.041	.035	NOT AVAILABLE	.126	.035
.11		.035	.041	.093	.033	.028		.090	.028
.21		.025	.028	.041	.023	.021		.040	.021
.30		.013	.015	.013	.014	.013		.013	.014
.41		.005	.005	.002	.006	.005		.002	.006
.50		.001	.001	.0001	.002	.002		.0002	.003
.60		0	.0002	0	.0004	.0004		0	.0007

TABLE 12

COMPARISON BETWEEN EXPERIMENTAL AND COMPUTED VELOCITY PROFILES, CASE C

VELOCITY (ft/sec)

R (in.)	z = 4" Initial Exper. Profile	z = 5" Exper.	z = 5" TRIAL 1	z = 5" TRIAL 2	z = 5" TRIAL 3	z = 7" Exper.	z = 7" TRIAL 1	z = 7" TRIAL 2	z = 7" TRIAL 3
0	1583	1462	1394	1516	1405	1345	1360	1469	1359
.11	1400	1360	1371	1393	1366	1316	1356	1389	1355
.21	1328	1332	1344	1331	1347	1327	1352	1338	1354
.30	1340	1353	1344	1340	1348	1347	1352	1344	1356
.41	1362	1370	1360	1362	1360	1365	1361	1361	1363
.50	1364	1361	1368	1366	1369	1383	1370	1368	1371
.60	1380	1383	1380	1380	1380	1384	1381	1380	1381

R (in.)	z = 8" Exper.	z = 8" TRIAL 1	z = 8" TRIAL 2	z = 8" TRIAL 3	z = 9" Exper.	z = 9" TRIAL 1	z = 9" TRIAL 2	z = 9" TRIAL 3
0	1339	1356	1454	1356	1336	NOT AVAILABLE	1444	1355
.11	1337	1355	1384	1355	1318		1383	1355
.21	1335	1353	1338	1355	1316		1339	1356
.30	1352	1355	1345	1358	1320		1345	1359
.41	1361	1362	1361	1364	1337		1360	1366
.50	1351	1371	1368	1372	1368		1368	1372
.60	1376	1381	1380	1381	1381		1380	1380

TABLE 13

COMPARISON OF E_d OBTAINED FROM SMOOTHED DATA VERSUS THAT OBTAINED FROM COSINE FITS, CASE A

E_d (ft^2/sec)

z (in.) / R (in.)	OBTAINED USING SMOOTHED INTERPOLATION DATA						OBTAINED USING COSINE FITS					
	3.0	5.0	6.0	7.0	8.0	9.0	3.0	5.0	6.0	7.0	8.0	9.0
.007	2.41	.10	0*	.08	.30	.02	.56	.69	1.02	.57	.77	.19
.013	2.32	.19	0	.14	.41	.04	.52	.65	.94	.54	.71	.18
.033	1.16	.41	0	.32	.54	.09	.52	.63	.92	.54	.72	.20
.046	.96	.52	0	.42	.58	.12	.53	.63	.91	.54	.73	.22
.065	.85	.65	11.9	.56	.62	.19	.53	.61	.90	.55	.75	.25
.078	.81	.70	4.5	.63	.65	.25	.54	.61	.89	.56	.76	.28
.091	.79	.74	2.5	.70	.68	.33	.55	.60	.87	.58	.76	.31
.104	.76	.77	1.5	.76	.70	.41	.56	.59	.86	.59	.76	.34
.124	.72	.78	1.0	.82	.72	.53	.57	.58	.85	.61	.74	.39
.137	.70	.77	.97	.86	.74	.60	.58	.58	.84	.63	.73	.43
.150	.68	.76	.90	.89	.74	.70	.60	.58	.84	.66	.71	.48
.163	.65	.74	.82	.90	.74	.79	.61	.58	.84	.69	.69	.53
.182	.61	.69	.72	.91	.73	.90	.63	.59	.84	.75	.65	.64
.195	.58	.66	.67	.91	.72	.96	.65	.61	.84	.81	.62	.75
.247	.57	.65	.61	.74	.71	.86	.78	.74	.93	1.3	.50	2.4

* These zero values occurred because $\overline{Y}$ at r = 0.125 in. was only 4% less than that at r = 0, instead of from 10 to 25% lower as occurred for all other profiles.

TABLE 14

COMPARISON OF ξ OBTAINED FROM SMOOTHED DATA VERSUS THAT OBTAINED FROM COSINE FITS, CASE A

ξ (lbm/ft-sec)

z(in) / R(in.)	OBTAINED USING SMOOTHED INTERPOLATED DATA						OBTAINED USING COSINE FITS					
	3.0	5.0	6.0	7.0	8.0	9.0	3.0	5.0	6.0	7.0	8.0	9.0
.007	.087	.006	0*	.006	.023	.002	.020	.041	.073	.042	.060	.015
.013	.083	.012	0	.011	.032	.003	.019	.039	.068	.040	.055	.014
.033	.042	.025	0	.024	.042	.007	.019	.038	.066	.040	.056	.016
.046	.035	.032	0	.032	.045	.010	.019	.038	.066	.040	.057	.017
.065	.031	.040	.856	.042	.049	.016	.020	.038	.065	.042	.058	.020
.078	.030	.044	.326	.048	.051	.020	.021	.038	.064	.042	.059	.022
.091	.029	.047	.180	.053	.053	.026	.021	.038	.064	.044	.060	.025
.104	.029	.049	.108	.058	.055	.033	.022	.038	.064	.045	.060	.027
.124	.028	.051	.076	.064	.058	.043	.024	.038	.063	.047	.059	.032
.137	.028	.051	.071	.067	.059	.049	.025	.039	.063	.049	.058	.035
.150	.028	.051	.067	.069	.060	.057	.026	.039	.064	.052	.057	.039
.163	.028	.050	.062	.071	.060	.066	.028	.040	.064	.055	.056	.044
.182	.027	.049	.055	.073	.060	.075	.031	.042	.065	.060	.053	.054
.195	.027	.047	.051	.073	.060	.080	.033	.044	.066	.065	.051	.063
.247	.033	.051	.050	.062	.060	.073	.046	.058	.076	.110	.042	.200

* These zero values occurred because $\overline{Y}$ at r = 0.125 in. was only 4% less than that at r = 0, instead of from 10 to 25% lower as occurred for all other profiles.